

1 **Extreme** warming rates affecting alpine areas in SW Europe deduced from algal
2 lipids 

3
4 Antonio García-Alix^{1,2,3*}, Jaime L. Toney², Gonzalo Jiménez-Moreno¹, Carmen Pérez-
5 Martínez⁴, Laura Jiménez⁴, Marta Rodrigo-Gámiz¹, R. Scott Anderson⁵, Jon Camuera⁶,
6 Francisco J. Jiménez-Espejo³, Dhais Peña-Angulo⁷, María J. Ramos-Román⁶

7
8
9 ¹ Department of Stratigraphy and Paleontology, University of Granada, Granada, 18072,
10 Spain.

11 ² School of Geographical and Earth Sciences, University of Glasgow, Glasgow, G12
12 8QQ, UK.

13 ³ Instituto Andaluz de Ciencias de la Tierra (IACT), CISC-UGR, Armilla, 18100, Spain.

14 ⁴ Department of Ecology and Institute of Water Research, University of Granada,
15 Granada, 18072, Spain.



16 ⁵ School of Earth and Sustainability, Northern Arizona University, Flagstaff, AZ 86011,
17 USA.

18 ⁶ Department of Geosciences and Geography, University of Helsinki, Helsinki, FI-00014,
19 Finland.

20 ⁷ Department of Geography, University of Zaragoza, Zaragoza, 50009 Spain.

21
22 * *Correspondence to:* Antonio García-Alix (agalix@ugr.es)

23

24 **Abstract.** Alpine ecosystems of the southern Iberian Peninsula are among the most
25 vulnerable and the first to respond to modern climate change in southwestern Europe.
26 While major environmental shifts have occurred over the last ~1500 years in these alpine
27 **ecosystems**, only changes in the recent centuries have led to **abrupt environmental**
28 responses, but factors imposing the strongest stress have been unclear until now. To
29 understand these environmental responses, **this study**, for the first time, **has calibrated an**
30 **algal lipid-derived temperature proxy** (based on long-chain **alkyl** diols) to instrumental
31 historical data extending alpine temperature **reconstructions to 1500 years before present**.
32 These novel results highlight the enhanced effect of greenhouse gases on alpine
33 temperatures during the last ~200 years and the long-term modulating role of solar
34 forcing. This study also shows that **the warming rate** during the 20th century
35 (~0.18°C/decade) **double**  **that of** the last stages of the Little Ice Age (~0.09°C/decade),
36 even exceeding temperature trends of the high-altitude Alps during the 20th century. As a
37 consequence, temperature exceeded the pre-industrial **records** in the 1950s, be  one of
38 the major forcings of the enhanced recent change in the alpine ecosystems from southern
39 Iberia. Nevertheless, other factors reducing the snow and ice albedo (**e.g.**, atmospheric
40 deposition) may have influenced local glacier loss, since **almost** steady climate conditions
41 predominated from middle 19th century to the first decades of the 20th century.

42

43 **1. Introduction**



44

45 Global mean annual surface temperatures have risen by ~0.85°C from 1880 to
46 2012 and the recent decades have been the **warmest in** the Northern Hemisphere during
47 the Common Era ([IPCC, 2013](#)). This trend is alarming, since over the last decade
48 temperature records have been broken yearly. For example, in Spain the highest

49 temperatures ever recorded in September and July occurred in 2016 (45.5°C) and 2017
50 (46.9°C-47.3°C), respectively ([Spanish National Weather Agency - AEMet Open Data,](#)
51 [2019](#)). Increasing global temperatures are contributing not only directly to land and ocean
52 surface warming, but are also changing the global hydrological cycle through the
53 disturbance of atmospheric circulation patterns and moisture ([Easterling et al., 2000;](#)
54 [IPCC, 2013](#)). As a result, the term “global warming” is migrating towards recent “**climate**
55 **change**” in order to express the variety of modern climate extremes witnessed across the
56 world. The effects of modern global warming and associated climate change events may
57 be causing extreme environmental impacts, beyond what is recorded in the recent
58 geologic record ([Waters et al., 2016](#)). Hence, it is crucial to identify warming thresholds,
59 rates, and forcing mechanisms from past high-resolution temperature records to
60 understand modern climate change. It is especially important in fragile regions such as
61 high elevation ecosystems of the Mediterranean alpine **realm**, an environmentally
62 vulnerable biodiversity “Hot-Spot” ([Giorgi, 2006;](#) [Schröter et al., 2005](#)) where recent
63 climate change is affecting species richness and distribution ([Médail and Quézel, 1999;](#)
64 [Pauli et al., 2012](#)). Therefore, alpine wetlands in the Mediterranean region, such as the
65 ones from the Sierra Nevada in the southern Iberian Peninsula, are sensitive recorders of
66 changing climate and their sedimentological records archive the ecological and
67 biogeochemical responses to different environmental forcings ([Catalan et al., 2013](#)).

68

69 In order to contribute to a better understanding of recent climate change events in
70 these vulnerable areas, here, for the first time, we calibrate a recently developed algal
71 lipid-derived temperature proxy in an alpine lacustrine record that overlaps with
72 instrumental temperature time-series. This calibration allows the reconstruction of
73 temperatures in alpine areas of the southern Iberian Peninsula during the Common Era

74 when instrumental records are discontinuous or non-existent. Temperature-dependent
75 biomarkers, such as those produced by algae (alkenones) or bacteria/archaea (glycerol
76 dialkyl glycerol tetraethers: GDGTs) have been commonly used in a wide range of marine
77 records as quantitative paleothermometers, and their further application in lake
78 environments has widely increased in the last decade (e.g., [Castañeda and Schouten,
79 2011](#); [Colcord et al., 2015](#); [Foster et al., 2016](#); [Longo et al., 2018](#); [Theroux et al., 2010](#)).
80 Another promising type of algal lipid biomarkers, the long-chain alkyl diols (hereafter
81 LCDs), have also been assessed as temperature proxy in marine  as ([Rampen et al.,
82 2014b](#); [Rampen et al., 2012](#); [Rodrigo-Gámiz et al., 2014](#); [Rodrigo-Gámiz et al., 2015](#)).
83 Nevertheless, the relationship between LCDs and temperature has only been tentatively
84 tested in freshwater environments ([Rampen et al., 2014a](#)). In this regard, studies using
85 LCDs as (paleo)environmental proxies in marine environments (not just only for
86 temperature reconstructions) have increased in the last years, showing the potential of
87 LCDs as upwe  g proxies ([Rampen et al., 2008](#); [Versteegh et al., 1997](#); [Willmott et al.,
88 2010](#)), riverine inputs in marine settings ([de Bar et al., 2016](#); [Lattaud et al., 2017a](#); [Lattaud
89 et al., 2018a](#)), or nutrient proxies ([Gal et al., 2018](#)). Nevertheless, only a few studies have
90 tested the  s lacustrine archives of paleoproductivity ([Shimokawara et al., 2010](#)), past
91 rainfall anomalies ([Romero-Viana et al., 2012](#)), or temperatures ([Rampen et al., 2014a](#)),
92 among others. In any case, despite the great potential of LCDs for paleoenvironmental
93 reconstructions, a number of questions exist about the applicability of diols in high
94 latitude areas ([Rodrigo-Gámiz et al., 2015](#)), in freshwaters records ([Rampen et al., 2014a](#)),
95 and about the distribution and sources of the biological producers ([Balzano et al., 2018](#);
96 [Villanueva et al., 2014](#); [Yu et al., 2018](#)), among  rs.
97

98 The LCD distribution in marine environments shows significant correlations with
99 mean annual sea surface temperature through the ratio of the fractional abundances of C₂₈
100 1,13-diol, C₃₀ 1,13-diol, and C₃₀ 1,15-diol that are used in the Long chain Diol Index (LDI,
101 Eq. (1)) ([Rampen et al., 2012](#)). **The application of LCDs as a temperature proxy** is novel
102 in freshwater environments and only **two** preliminary calibrations based on **recent surface**
103 **sediments** have been **obtained using both mean annual air temperatures (weather station**
104 **data) and organic-derived temperature proxies** (GDGTs) ([Rampen et al., 2014a](#)). Here,
105 we improve the biomarker paleothermometry by establishing the first temperature
106 calibration for freshwater LCDs using a comparison with historical temperature records
107 for the last ~100 years. **Although this calibration can only be applied to the studied lake**
108 **at present, and perhaps to other alpine wetlands in the Sierra Nevada area,** these new data
109 support and reinforce the **promising** use of LCDs as a paleotemperature proxy in
110 freshwater environments.

111

112 Equation (1) $LDI = (F_{C_{30} 1,15\text{-diol}}) / (F_{C_{28} 1,13\text{-diol}} + F_{C_{30} 1,13\text{-diol}} + F_{C_{30} 1,15\text{-diol}})$
113 ([Rampen et al., 2012](#))

114

115 **1.1 Regional settings**

116

117 This paper focuses on the LCD record of two adjacent cores from Laguna de Río
118 Seco (LdRS), a small alpine lake (~0.42 ha and less than 3m of water depth) at 3020 masl
119 in the protected Sierra Nevada National Park, southern Spain (Fig. 1). Alpine Sierra
120 Nevada wetlands, including LdRS, are low primary production (oligo-mesotrophic)
121 systems and their biogeochemical cycles partially depends on aeolian nutrient supplies

122 (e.g., Saharan aerosol deposition), since catchment basins are small and barren in
123 nutrients ([Morales-Baquero et al., 2006](#); [Pulido-Villena et al., 2005](#); [Reche et al., 2009](#)).

124

125 Sierra Nevada is the southwestern-most mountain range in Europe, where latest
126 Pleistocene cirque glaciers carved the metamorphic (mica schist) bedrock in the highest
127 peaks ([Castillo Martín, 2009](#)). Massive glacier melting at the latest Pleistocene-Holocene
128 transition transformed the former glacial depressions into **lacustrine areas** ([Castillo](#)
129 [Martín, 2009](#)) that evolved gradually into either shallow lakes or peatlands around the
130 middle-to-late Holocene transition ([Garcia-Alix et al., 2017](#); [Jiménez-Espejo et al., 2014](#)).
131 Small glaciers re-appeared at the highest peaks of the Sierra Nevada in the 15th century,
132 during the Little Ice Age (LIA), and remained until the 20th century ([Oliva et al., 2018](#)).
133 The presence of these glaciers is observed in the sedimentary record in some alpine lakes
134 **and wetlands** in the Sierra Nevada as deposit of coarse sediments, like Laguna de la
135 Mosca **on the north face of the Sierra Nevada** ([Oliva and Gomez-Ortiz, 2012](#)). However,
136 these kinds of deposits have not been registered in LdRS (**south face of the Sierra**
137 **Nevada**), where the last 1500 years are characterised by continuous laminated clays and
138 bryophyte layers ([Anderson et al., 2011](#)). In an se, glacial effects have not caused any
139 disturbance on wetland sedimentation (e.g., erosion) **and** local alpine sedimentary records
140 show continuous sedimentation patterns ([Anderson et al., 2011](#); [García-Alix et al., 2012](#);
141 [Jiménez-Moreno and Anderson, 2012](#); [Jiménez-Moreno et al., 2013](#); [Mesa-Fernández et](#)
142 [al., 2018](#); [Oliva and Gomez-Ortiz, 2012](#); [Ramos-Román et al., 2016](#)). **Conversely, an**
143 **increase in sedimentation rates have been detected in the last ~200 years, probably**
144 **resulting from the waning stages of the LIA** ([Oliva and Gomez-Ortiz, 2012](#)) **and enhanced**
145 **human activities in the alpinos areas of Sierra Nevada during the 19th** ([García Montoro et](#)
146 [al., 2016](#); [Titos Martínez, 2019](#); [Titos Martínez and Ramos Lafuente, 2016](#)) **and 20th**

147 ([Jiménez et al., 2015](#)) centuries. These high-sedimentation rates did not affect the natural
148 responses of the local algal communities to environmental variables such as temperature,
149 but with a primary effect of dilution of algal compounds (e.g., chlorophylls and labile
150 carotenoids) in the sediments ([Jiménez et al., 2015](#)).

151

152 During the 20th century this sensitive alpine region of southern Iberia has
153 experienced significant impacts from modern climate change as evidenced, for example,
154 by the first permanent European glacier loss there during the first half of the 20th century
155 ([Grunewald and Scheithauer, 2010](#)) and the extreme permafrost reduction during recent
156 decades ([Oliva and Gomez-Ortiz, 2012](#)). This melting supplied a large volume of
157 freshwater ([Jiménez et al., 2019](#)) that boosted the water availability in the area and the
158 occasional development of local aquatic environments, contrasting with the general
159 environmental aridification trend observed throughout the 20th century ([Garcia-Alix et](#)
160 [al., 2017](#); [Jiménez et al., 2019](#); [Ramos-Román et al., 2016](#)).

161

162 The sedimentary archive of LdRS has been selected for this study in order to 1)
163 improve the freshwater LCD paleothermometry by proposing a new temperature
164 calibration for freshwater LCDs in the alpine wetlands of the Sierra Nevada area, 2)
165 reconstruct temperatures beyond the instrumental record in a site at the leading edge of
166 changing climate, 3) assess the role of different radiative forcing (e.g., solar radiation or
167 greenhouse gas concentrations) on temperature change in alpine wetlands of the
168 southwestern Europe during the Common Era, and 4) understand the responses to recent
169 climate change in this highly sensitive environment.

170

171 **2. Materials and methods**

172

173 **2.1. Sediment sampling**

174

175 Two sediment cores were taken at the deepest part of LdRS, an alpine lake at 3020
176 masl in the Sierra Nevada (southern **Iberian Peninsula**) (Fig. 1). A long sediment core
177 (150 cm) was retrieved in 2006 (LdRS lgc). A short sediment core of 16 cm was collected
178 in 2008 (LdRS shc) using a slide-hammer gravity corer (Aquatic Research Instruments,
179 Hope, Idaho, USA). Independent age models were performed in each sediment core to
180 avoid potential correlation problems caused by changes in the sedimentation rates
181 between both coring sites (Fig. 1c) and different sampling dates (2006-LdRS lgc and
182 2008-LdRS shc). The age model of LdRS lgc is based on ^{210}Pb and ^{137}Cs in the uppermost
183 part (first 15 cm), and ^{14}C analyses in older sediments ([Anderson et al., 2011](#)). The age
184 model of the LdRS shc is based on gamma spectroscopy by measuring the ^{210}Pb , ^{137}Cs ,
185 and ^{226}Ra radionuclides in the first ~14 cm, and afterwards the age was extrapolated to
186 the core bottom (16 cm) ([Jiménez et al., 2019](#); [Jiménez et al., 2018](#)). Both records show
187 that the sediment accumulation rate for the uppermost 15-16 cm ranges between **0.09** and
188 0.13 cm/yr ([Anderson et al., 2011](#); [Jiménez et al., 2018](#)), with lower sedimentation rates
189 below this depth (~0.008 cm/yr) ([Anderson et al., 2011](#)). Ages models show that the LdRS
190 shc extends back to ~200 years with a sample resolution ranging from 5 to 7 years (high-
191 resolution) ([Jiménez et al., 2019](#); [Jiménez et al., 2018](#)). In the case of the LdRS lgc, the
192 section studied in this paper covers the last ~1500 years with a lower sample resolution.
193 In this case, the sample resolution is around 6-7 years in the first 10 cm, and from 24 to
194 150 years in older samples ([Anderson et al., 2011](#)).

195

196 **2.2. Geochemical analyses**

197

198 Thirty-two sediment samples were collected consecutively every 0.5 cm along
199 LdRS shc and **twenty-one** samples in the first 22 cm of LdRS lgc. The samples were
200 freeze-dried and homogenized. The total lipid content was extracted from the sediment
201 samples using a Thermo Scientific™ Dionex™ ASE™ 350 Accelerated Solvent
202 Extractor system at 100°C and 7×10^6 Pa using a mixture of dichloromethane (DCM) and
203 methanol (9:1, v:v). Afterwards, the neutral fraction was separated by means of
204 aminopropyl-silica gel chromatography using DCM:isopropanol (1:1, v:v). This neutral
205 fraction was subsequently eluted with hexane, DCM, ethyl acetate:hexane (25:75, v:v),
206 and methanol through a 230-400 mesh/35-70 micron silica-gel chromatographic column,
207 in order to obtain four neutral sub-fractions (N1-N4). Long chain diols were obtained in
208 the third neutral fraction (N3, alcohol fraction), which was derivatised by bis-
209 (trimethylsilyl) trifluoroacetamide (BSTFA) before running the analyses. 30µL of
210 BSTFA and 40µL of pyridine were added to each N3 fraction and heated at 80°C for 2
211 hours. When vials were at room temperature, a volume between 140 µl and 220 µl of
212 DCM was added to each sample. Firstly, the derivatised N3 fractions were analysed with
213 a Gas Chromatography with Flame-Ionization Detector (GC-FID Shimadzu 2010). **An**
214 **external standard of cholesterol was measured every five samples in order to estimate the**
215 **proper concentration for mass spectrometry analyses. The sample at 19.5 cm depth in the**
216 **long core was discarded because its concentration was below detection limits.**
217 Subsequently, **the N3 fractions** were measured in a Shimadzu QP2010-Plus Mass
218 Spectrometer interfaced with a Shimadzu 2010 GC using a scan mode between m/z 50 –
219 650, in order to obtain a general picture of the mass spectrum of the samples and **the**
220 **specific retention times where the C₂₈, C₃₀, and C₃₂ diols eluted. Afterwards, samples**
221 **where re-analysed** on the basis of a Selected-Ion Monitoring mode (SIM), selecting the

222 characteristic fragment ions of the most important long chain diols, i.e., m/z 299, 313,
223 327, and 341 ([Rampen et al., 2012](#); [Versteegh et al., 1997](#)) and the specific retention time
224 window to identify the C₂₈, C₃₀, and C₃₂ diols with the mid-chain alcohol positioned at
225 carbon 13, 14 or 15. Fractional abundances of the C₂₈ 1,13-diol, C₃₀ 1,13-diol, C₃₀ 1,15-
226 diol were used in Eq. (1) to calculate the Long chain Diol Index (LDI) ([Rampen et al.,](#)
227 [2012](#)). Fractional abundances of C₂₈ 1,13-diol, C₃₀ 1,13-diol, C₃₀ 1,15-diol and C₃₂ 1,15-
228 diol were used to characterise the potential diol source (e.g., marine, lacustrine, or specific
229 algae groups) ([Lattaud et al., 2018a](#); [Rampen et al., 2014a](#)). Fractional abundances of the
230 C₂₈ and C₃₀ 1,14-diols were measured only in the short core in order to assess their
231 potential relationship with temperatures ([Rampen et al., 2014b](#)). The presence of the C_{32:1}
232 1,15-diol has also been tested, but it was only identified in some samples from the short
233 core at very low concentrations, thus is not included in this study.

234

235 **2.3. Reference temperature time-series for LCD temperature calibrations**

236

237 Generating an accurate temperature calibration based on LCDs in alpine wetlands
238 from the Sierra Nevada area is challenging, because there is a lack of long and continuous
239 temperature time-series at such high elevations. The meteorological observatories at the
240 Sierra Nevada ski resort (ranging in elevation from 2500 to 3020 masl) only provided
241 discontinuous temperature records from 1965 to 2011 ([Observatorio del cambio global](#)
242 [de Sierra Nevada, 2016](#); [Spanish National Weather Agency - AEMet Open Data, 2019](#))
243 that show a significant correlation ($r > 0.95$; $p < 0.0001$) with low elevation temperature
244 time-series (Table S1, S2). Therefore, a potential way to obtain a LCD-based temperature
245 calibration is by means of the correlation of LCD data with long and reliable historical

246 temperature time-series at nearby lower elevation areas, followed by a correction for the
247 altitudinal effect on temperatures.

248

249 The three weather observatories in the Granada area, at the foothills of the Sierra
250 Nevada, only provide reliable temperature data from the 1970s onwards ([Spanish
251 National Weather Agency - AEMet Open Data, 2019](#)), which is a short-period for an
252 accurate down-core proxy calibration. Temperature time series from the 1970s
253 backwards have been reconstructed using statistical models (e.g., [Gonzalez-Hidalgo et al.,
254 2015](#)), showing a good correlation with the LDI and with the relative abundance of the
255 C₂₈ 1,13-, C₃₀ 1,13-, and C₃₂ 1,15-diols, with a weaker correlation for the C₃₀ 1,15-diol
256 (Table S3). However, these correlations are lower than the ones obtained from Sevilla-
257 Tablada and Madrid-Retiro observatories. These observatories registered longer and
258 more reliable temperature data than those obtained in Granada observatories, which are
259 likely biased by the quality of the reconstructed temperature data. Therefore, after testing
260 the correlations between LCDs and different low elevation observatories (Table S3), we
261 decided to develop the LCD-based temperature calibrations against the temperature time-
262 series from Sevilla-Tablada and Madrid-Retiro observatories. These observatories show
263 the best correlations with the LCD data, in addition to being the most reliable and longest
264 temperature time-series in the region (see Table S3 for further explanations and Fig. 1a
265 for the location of these low-elevation observatories).

266

267 Another question to clarify in the study records before selecting the reference
268 temperature time-series for the LCD calibration is the potential seasonal effect on the
269 LCD distributions, since different studies have shown diverse relationships between
270 annual or seasonal temperatures and the LCDs. For example, good correlations have been

271 found in marine environments between the fractional abundances of LCDs (expressed as
272 LDI in all the cases) and annual ([Rampen et al., 2012](#)), winter and annual ([Smith et al.,
273 2013](#)), or autumn and annual sea surface temperatures ([Lattaud et al., 2018b](#)). Despite
274 fewer studies on the LCD distribution in freshwater environments, Rampen et al. (2014a)
275 found a good correlation between the LCD distributions in a suite of lake surface
276 sediments and mean summer lake temperatures (deduced from GDGTs). Nevertheless,
277 the direct correlation between these LCD distributions and annual or seasonal air
278 temperatures was weaker, probably due to the location of the weather observatories with
279 respect to each study area. Villanueva et al. (2014) also investigated this seasonal effect
280 and detected changes in the LCD distribution throughout the year in the water column
281 and surface sediments from an African lake that could be either related to successive and
282 different LCD-producer blooms or seasonal variations in the LCD production by a unique
283 source. Both scenarios might affect LCD-based temperature reconstructions.

284

285 Considering all these constrains to select the best temperature time-series to
286 establish an accurate LCD-based temperature calibration, the most rigorous approach for
287 the studied alpine site would consider annual and monthly water and/or air temperatures
288 of the catchment basin at 3020 masl, as well as, the periods of the year when the LCDs
289 are produced, but these data are not available so far. Thus, the effect of seasonality has
290 been estimated by means of the comparison with reliable seasonal long temperature time-
291 series from lower elevation sites. In this regard, seasonal air temperatures for the last ~100
292 years registered in Madrid and Sevilla observatories correlate with the LCD distributions
293 (with a weaker correlation for the C₃₀ 1,15-diols) and the LDI ($0.9 > r > 0.6$; $p < 0.001$).
294 Nevertheless, this correlation is generally lower than the one obtained when considering
295 only mean annual air temperatures (MAAT) (i.e., in the case of the LDI vs MAAT $r = 0.9$;

296 $p < 0.0001$). Since warm temperatures influence the algae growth in the studied area
297 ([Carrillo et al., 1991](#); [Sánchez-Castillo, 1988](#)), we would expect a higher correlation
298 between LCDs and mean seasonal air temperatures from the warmer months (MWAT:
299 May-September), which is potentially the LCD production season, but this correlation is
300 lower than the annual ones in the case of the LDI (LDI vs MWAT $0.8 > r > 0.7$; $p < 0.0001$)
301 (Table S3, S4). A similar pattern is observed when annual and warm season temperatures
302 are compared with the fractional abundances of the C₂₈ 1,13-, C₃₀ 1,13-, C₃₀ 1,15-, and
303 C₃₂ 1,15-diols (Table S3). Consequently, in view of 1) the fact that this is the first attempt
304 at a freshwater LCD-based temperature calibration in this area; 2) there exists a high
305 correlation between the different instrumental time-series of regional air temperatures
306 (seasonal vs annual), and 3) the best correlations (normal and detrended) between the
307 LCD distributions and temperatures are obtained when using MAAT (Tables S3, S4), we
308 use MAAT for the LCD-based temperature calibrations in this study. Nevertheless,
309 further work, including a monitoring program for monthly air temperatures in the
310 catchment area and water temperatures at the lake, as well as, suspended particulate
311 matter and sediment trap studies, is needed to better understand the seasonal LCD
312 production and the biological sources, providing more constrains to improve the current
313 LCD-based temperature calibration.

314

315 Two groups of reference temperature time-series at 3020 masl, based on the same
316 batch of data, have been estimated in order to overcome the scarcity of high-elevation
317 temperature time-series in the Sierra Nevada and obtain a reliable mean LCD-based
318 temperature calibration: 1) based on the elevational gradient between low and high
319 elevation observatories and 2) based on the direct correlation between temperature time-
320 series from Madrid and Sevilla observatories and that at 3020 masl (Cetursa 5

321 observatory) in the Sierra Nevada, which is near LdRS and at the same elevation (Table
322 S1).

323

324 Reference temperature time-series 1: The environmental lapse rate
325 ($\Delta_{\text{temperature}}/\Delta_{\text{elevation}}$ in °C/m) between lower elevation observatories (with long
326 temperature time-series: Granada, Sevilla, and Madrid) and those from Sierra Nevada at
327 higher elevation (with shorter temperature time-series: Albergue, and Cetursa 1, 3 and 5)
328 has been estimated in order to correct the elevational gradient between them (more than
329 2200 m: Table S1). Due to few annual data points from high elevation sites, monthly and
330 annual (twelve continuous months) environmental lapse rates were calculated to compare
331 both datasets. The calculated temperature shifts between the reference low elevation
332 observatories and LdRS site at 3020 masl, worked out from Fig. S1 equations (Table S5),
333 was applied to the temperature time-series from Madrid and Sevilla for the last ~100 years
334 in order to obtain two reference temperature reconstructions (from 1908 to 2008 CE) at
335 3020 masl: reference temperature time-series 1a (from Madrid data), and reference
336 temperature time-series 1b (from Sevilla data).

337

338 Reference temperature time-series 2: The direct comparison between Madrid and
339 Sevilla temperatures and those from the observatory Cetursa 5 (3020 masl) by means of
340 ordinary least square regressions has given rise to two equations (Fig. S2a and b) that
341 allow the reconstruction of temperature time-series at 3020 masl from 1908 to 2008:
342 reference temperature time-series 2a (from Madrid data), and reference temperature time-
343 series 2b (from Sevilla data).

344

345 As a result, we have obtained four reference temperature time-series at 3020 masl
346 where the effect of the altitudinal difference between low elevation observatories (Madrid
347 and Sevilla) and LdRS have been corrected by two different methods. Consequently,
348 these four reference temperature series are highly similar, showing a certainly high
349 correlation ($r>0.98$; $p<0.0001$), without significant difference between the sample
350 medians (deduced from a Kruskal-Wallis test), and very low standard deviation between
351 samples from the same time interval (SD 0.2).

352

353 3. Results

354

355 3.1. Long chain diols in the LdRS records

356

357 Six main LCD isomers have been identified and relatively abundances analysed
358 in the LdRS cores: C₂₈ and C₃₀ 1,13-diols, C₂₈ and C₃₀ 1,14-diols, and C₃₀ and C₃₂ 1,15-
359 diols. Their relative abundance changes through time in both records, but the C₃₂ 1,15-
360 diol is the predominant isomer in most of the samples. Nevertheless, the relative
361 abundance of the C₃₂ 1,15-diol drops abruptly (relative abundances between 25% and
362 40%) during the LIA, contrasting with a relative increase in the C₂₈ and C₃₀ 1,13-diols
363 (Fig. 2). This switch in the most abundant isomers can be read as either a change in the
364 LCD producers or an adaptation to colder temperatures of the same organism, and thus
365 affecting the LCD production. Conversely, the C₂₈ and C₃₀ 1,14-diols show the lowest
366 relative abundances ($1.3 \pm 0.4\%$ and $1.8 \pm 0.3\%$, respectively). They were only quantified
367 in the short core to assess their potential application as paleothermometer in LdRS.
368 Although they show a good correlation with temperatures (C₂₈ 1,14-diol: $0.66 > r > 0.45$
369 $p < 0.04$; C₃₀ 1,14-diol: $-0.82 < r < -0.53$ $p < 0.02$), their low relative abundance, very close to

370 the detection limit, together with a different biological source ([Sinninghe Damsté et al.,](#)
371 [2003](#)), preclude us from including them in the temperature calibration, and therefore, in
372 the discussion of this study. Consequently, the interpretations in this paper are only
373 focused on the distribution pattern of the relative abundances of the main LCDs in LdRS:
374 C₂₈-C₃₀ 1,13-diols and C₃₀-C₃₂ 1,15-diols.

375

376 The relative abundances of these four isomers in LdRS correlate well in both short
377 and long cores, only C₃₀ 1,15-diol showing weaker correlations with the other isomers
378 (Table S6). Overall, C₂₈ and C₃₀ 1,13-diols show opposite trends to those from the C₃₀
379 and C₃₂ 1,15-diols. Their general trends for the last ~100 years seem to be influenced by
380 the temperature oscillations at 3020 masl (Table S7): the C₂₈ and C₃₀ 1,13-diols display a
381 negative correlation with temperatures ($r < -0.7$ $p < 0.0001$) and the C₃₂ 1,15-diol a positive
382 one ($r > 0.8$ $p > 0.0001$). Although the C₃₀ 1,15-diol also shows a positive relationship with
383 temperatures, this correlation is weak ($r > 0.3$ $p > 0.0001$). Accordingly, the LDI values
384 from LdRS for the last ~100 years show a significant correlation ($r > 0.9$ $p > 0.0001$) with
385 the reference temperature time-series at 3020 masl (Table S7).

386

387 The different diol isomers in LdRS also show good agreement with general
388 temperature trends during the last ~1500 years. The C₃₀ and C₃₂ 1,15-diols depict a
389 positive relationship with temperatures, whereas the C₂₈ and C₃₀ 1,13-diols display a
390 negative one. Thus, the LDI record obtained from the C₂₈-C₃₀ 1,13-diols, and C₃₀ 1,15-
391 diol also show important fluctuations during the last ~1500 years, in agreement with the
392 general temperature trends of the Common Era (CE). More specifically, LDI values in
393 the LdRS Igc range from ~0.23 to 0.05 from ~400 to 1900 CE, with maximum and
394 minimum values recorded at ~930 and ~1690 CE, respectively (Fig. 3). These changes

395 are coeval with the minimum temperatures of the LIA and the maximum temperatures of
396 the Medieval Climate Anomaly (MCA). LDI fluctuations were extremely abrupt during
397 the 20th century, ranging from 0.10 to 0.31 in the lowest resolution LdRS lgc record and
398 from 0.13 to 0.32 in the highest resolution LdRS shc record. These minimum and
399 maximum values were reached in both cases during the first and last decades of the 20th
400 century, respectively (Fig. 3).

401

402 **3.2. LCD temperature calibration**

403

404 A total of twenty-six samples from both short and long LdRS cores ranging in age
405 from 1908 to 2008 were selected to perform the LCD-based temperature calibration,
406 along with the two groups of reference temperature time-series at 3020 masl. Since
407 sedimentary samples used in the calibration have a time averaging between 5 and 7 years,
408 a mean of the historical temperatures covering the same time averaging of each sample
409 was calculated.

410

411 Eight different calibrations have been performed: five using the LDI, one using a
412 multiple linear regression of the relative abundances of C₂₈ 1,13-diol, C₃₀ 1,13-diol, and
413 C₃₀ 1,15-diol (following [Rampen et al., 2014a](#)) (MLR calibration 1 hereafter), one using
414 multiple linear regressions of the ratios of the relative abundances of LCDs with positive
415 (even weak) correlation with temperature against the ones with negative correlation (C₃₀
416 1,15- / C₂₈ 1,13-diols; C₃₀ 1,15- / C₃₀ 1,13-diols; C₃₂ 1,15- / C₂₈ 1,13-diols; and C₃₂ 1,15-
417 / C₃₀ 1,13-diols) (MLR calibration 2 hereafter), and one using multiple linear regressions
418 of the ratios of the relative abundances of C₃₀ 1,15- / C₂₈ 1,13-diols and C₃₀ 1,15- / C₃₀

419 1,13-diols (MLR calibration 3 hereafter). The statistics and the equations for the MLR
420 calibrations 1, 2, and 3 are described in the Table S8.

421

422 In the case of the LDI, ordinary least square regressions were run between the four
423 reference temperature time-series at 3020 masl and the LDI record from LdRS shc and
424 lgc, resulting in four calibration equations (Fig. S3). The slopes of these four equations
425 range from 8.2 to 10.2. The LDI-derived temperatures from the reference time-series 2
426 show the highest values for the last ~100 years, whereas the minimum values are mainly
427 shown by the ones calculated with the reference time-series 1. The difference between
428 the four LDI-derived temperatures for the last ~100 years is low, with a standard deviation
429 lower than 0.13. The standard error of these four individual calibrations ranges from 0.18
430 to 0.23°C, and the maximum residual is ~0.8°C. However, due to the uncertainty of
431 establishing an accurate temperature time-series at 3020 masl, LDI-derived temperature
432 values from these LDI individual calibrations have been used to determine the range of
433 the variation (minimum and maximum temperature values) for each point, and an
434 additional calibration, summarising the relationship between LDI and the four reference
435 temperatures at 3020 masl has been performed. The obtained 104 combinations of LDI
436 and temperature data provided an equation representing the average relationship between
437 MAAT and LDI (Eq. (2); Fig. 4a). Since this is a summary of the four temperature time-
438 series, the residual errors include the residual errors of the individual LDI calibrations
439 (Fig. S3). The residual errors of this average temperature calibration, according to both
440 the LDI-reconstructed temperatures and the reference temperature time-series, are lower
441 than 0.8°C (similar to the four individual LDI calibrations), with the standard error of
442 0.28°C. The histogram showing the frequency of the residuals reveals that the ~85% of
443 the residuals range from 0.4 to -0.4°C. This percentage is slightly lower (~62%) when the

444 residual interval is established between 0.2 and -0.2°C (Fig. 4b). Only one data point from
445 1973 among the 104 data combination may be an outlier since it shows a residual 2.5
446 times higher than the residual standard deviation.

447

448 Equation (2) $MAAT (^{\circ}C) = 9.147 \times LDI - 0.243$ (n = 26 x 4; $r^2 = 0.79$)*

449 * n = 26 LDI values plotted against four reference temperature time-series providing a
450 total of 104 combinations.

451

452 All the calibrations (LDI and MLR calibration 1, 2, and 3) show good correlation
453 with temperatures (Fig. 4 for LDI and Table S8 for MRL calibrations 1, 2, and 3). The
454 obtained temperatures from the average LDI calibration and those using multiple linear
455 regressions depict very similar trends in both cores (Fig. S4; $r > 0.96$; $p < 0.0001$).
456 Nevertheless, the correlation is slightly lower ($r > 0.82$; $p < 0.0001$) for the results from
457 MLR calibration 1 in the long core. In addition, some inconsistencies come up in the
458 reconstructed temperatures from MLR calibration 1: in general, temperatures tend to be
459 lower than those from the other calibrations, giving rise to negative annual values during
460 the LIA. This would be highly unlikely since under this scenario the lake would have
461 stayed frozen all year round, with little or no sedimentation occurring. Temperature
462 reconstructions using MLR calibrations 2 and 3 take the advantage of the ratios of isomers
463 with positive vs negative relationship with temperatures. The results are similar to the
464 ones obtained with the LDI, except for the LIA. Nevertheless, we discarded MRL
465 calibration 2 as it also uses the C₃₂ 1,15-diol, whose relationship with temperature is not
466 clear, only reporting a positive correlation in some culture studies (Rampen et al., 2014b).
467 MRL calibration 3 provides the most similar results to those from the LDI, especially
468 comparing the temperature anomalies of both records with respect to the last 30 years of

469 the record, showing differences of less than $\sim 0.1^{\circ}\text{C}$. However, this difference increases
470 ($\sim 0.3^{\circ}\text{C}$) in the LIA. As this is the first study of LDI in sedimentary records from alpine
471 lakes of the Sierra Nevada area, we have opted for a conservative solution following the
472 LDI temperature calibration. The temperature reconstructions from MRL calibration 1,
473 2, and 3 will only be mentioned when needed in the discussion.

474

475 The application of the obtained calibration to the LDI values of LdRS (Eq. 2)
476 produced the first temperature reconstruction for the Common Era in this alpine area (Fig.
477 3). In order to estimate the real magnitude of temperature variations during this period,
478 the mean annual air temperature anomaly (MAATA $^{\circ}\text{C}$) has been calculated with
479 reference to the annual MAAT of the last 30 years of the record (2008-1979). The lowest
480 temperatures were recorded between ~ 1600 and ~ 1780 CE, with a temperature anomaly
481 ranging from ~ -1.9 to $\sim -2.2^{\circ}\text{C}$. These temperature anomalies only reached positive
482 values after 1998 (Fig. 3).

483

484 **4. Discussion**

485

486 **4.1. Long chain diol distribution in alpine lakes from southern Iberia**

487

488 The distribution pattern of the main LCDs in LdRS (C_{28} , C_{30} 1,13- and C_{30} , C_{32}
489 1,15-diols) could help us decipher the potential biological producers. There is a high
490 percentage of the C_{32} 1,15-diol, which is one of the main features observed in freshwater
491 environments ([Lattaud et al., 2018a](#); [Rampen et al., 2014a](#)) (Fig. 2, S5). Another relevant
492 feature of the distribution of the LCDs in LdRS is the low and constant relative abundance
493 of the C_{30} 1,15-diol ($6.5 \pm 1.5\%$) throughout the LdRS records (Fig. 2), agreeing with the

494 range of the most probable distribution of C₃₀ 1,15-diol in marine algae (Fig. S5; Table
495 S9). This feature is not common in marine or lake sediments ([de Bar et al., 2016](#); [Lattaud
496 et al., 2017a](#); [Rampen et al., 2014a](#)), resulting in an almost unique area for LdRS isomers
497 (most specifically C₂₈ 1,13-, C₃₀ 1,15-, and C₃₂ 1,15-diols) when comparing with
498 literature data in a ternary diagram (Fig. 2). Conversely, the distribution of both C₂₈ and
499 C₃₀ 1,13-diols usually shows similar patterns as other freshwater samples ([Lattaud et al.,
500 2018a](#); [Rampen et al., 2014a](#)) (Fig. 2, S5, Table S9). A Kruskal-Wallis ANOVA test was
501 used to assess whether the distribution of the main LCDs in LdRS and from other sources
502 (e.g., marine, freshwater, algal culture) were statistically different. Results point towards
503 no significant differences between the whole LCD distribution in LdRS and the other
504 sources. Nevertheless, the Kruskal-Wallis test found significant differences among
505 individual isomers of the different sources (including LdRS). Subsequently, a Mann-
506 Whitney U test was performed to compare pair of groups (individual isomers from LdRS
507 vs individual isomers from source 1, 2, and so on), finding significant differences among
508 most of them (Table S9). All these evidences suggest that the LCD distribution in the
509 LdRS might differ from those of previous studies published to date and the potential
510 biological producers at LdRS would be thus uncertain.

511

512 Eustigmatophyceae algae (e.i. *Vischeria* sp., *Eustigmatos* sp.) have been
513 commonly proposed as the main diol producers in freshwater environments dominated
514 by a mix of C₂₈ 1,13-, C₃₀ 1,15-, and C₃₂ 1,15-diols ([Rampen et al., 2014a](#); [Villanueva et
515 al., 2014](#); [Volkman et al., 1999](#)). Moreover, a dominance of C₃₂ 1,15-diol has been
516 identified in families of Goniochloridaceae and Monodopsidaceae ([Lattaud et al., 2018a](#);
517 [Rampen et al., 2014a](#)). Nevertheless, planktonic algae communities are very simple in the
518 alpine Sierra Nevada wetlands ([Sánchez-Castillo, 1988](#)) and Eustigmatophyceae algae

519 have not been identified so far ([Barea-Arco et al., 2001](#); [Sánchez-Castillo, 1988](#)). Thus,
520 this study suggests that LCD producers in LdRS might be different from those identified
521 previously in other freshwater environments and algal culture studies, making the
522 potential source of LCDs even more complex than originally thought. Consequently, the
523 outcomes of this paper (i.e., the LCD-based temperature calibration) should not be
524 generally applied to other freshwater records unless they show a similar LCD distribution
525 as LdRS. Additional research combining lipids and 18S rRNA gene sequencing analyses
526 from suspended particulate matter, surface sediments, and sediment traps would be
527 needed to unravel the real biological sources of LCDs in these alpine wetlands.

528

529 **4.2. LdRS record in the environmental context of the Iberian Peninsula during the**

530 **Common Era**

531

532 Abrupt changes in temperature and precipitation have been depicted during the
533 last 2000 years in the Iberian Peninsula and surrounding marine areas ([Moreno et al.,](#)
534 [2012](#); [Sánchez-López et al., 2016](#)). Precipitation was highly variable, showing arid
535 conditions during the MCA, especially in southern Iberia, overall humid conditions
536 throughout the LIA (with a complex internal structure showing large variability in
537 humidity and extreme events), and arid conditions for the Industrial Period ([Moreno et](#)
538 [al., 2012](#); [Oliva et al., 2018](#); [Rodrigo et al., 1999](#); [Sánchez-López et al., 2016](#)), especially
539 in high elevation wetlands from southern Iberia ([Anderson et al., 2011](#); [Garcia-Alix et al.,](#)
540 [2017](#); [Jiménez-Espejo et al., 2014](#)).

541

542 Although the Early Middle Ages displayed a great temperature variability in the
543 Iberian Peninsula and surrounding marine sites ([Moreno et al., 2012](#); [Sánchez-López et](#)

544 [al., 2016](#)), three main stages have been identified for the last millennium deduced from
545 different proxies: a warm period throughout the MCA followed by cold temperatures
546 during the LIA, ending in an abrupt warming in the second half of the 20th century
547 ([Moreno et al., 2012](#); [Oliva et al., 2018](#); [Sánchez-López et al., 2016](#)). One of the proxies
548 used to reconstruct such temperature variations in continental areas of the Iberian
549 Peninsula has been tree ring data. Long tree ring temperature archives of the Iberian
550 Peninsula showed the same overall variations as the ones registered in LdRS, such as high
551 temperatures before 1250 CE ([Büntgen et al., 2017](#)), some temperature declines coeval
552 with solar minima during the LIA (e.g., the end of Spörer or Maunder Minima), as well
553 as a period of moderate-low temperatures from ~1850 to ~1940, followed by an
554 increasing temperature trend in the second half of the 20th century with several
555 temperature drops between ~1960 and ~1990 ([Büntgen et al., 2017](#); [Tejedor et al., 2017](#)).
556 Nevertheless, the warming documented from the LCD-derived temperatures in the last
557 stages of the LIA is more pronounced in the LdRS record. The same overall trends have
558 been observed in European summer temperatures deduced from tree ring records
559 ([Luterbacher et al., 2016](#)) (Fig. 5b, d, and 6b, c). Surprisingly, tree ring data from the
560 Pyrenees and other Iberian areas show minor temperature variations, and even a slight
561 temperature decrease from ~2000 to 2008 similar to the one observed in the LCD-derived
562 temperatures from the LdRS record (Fig. 4c). This temperature stabilization at the
563 beginning of the 21st century is coeval with globally reduced warming rates over the
564 2001–2014 period ([Fyfe et al., 2016](#)).

565

566 Contrasting with these continental temperature reconstructions, high-resolution
567 sea surface temperature (SST) estimations from marine sites surrounding the Iberian
568 Peninsula, such as those derived from alkenones ($U^{K'_{37}}$) in the Tagus Delta (Iberian

569 Atlantic Margin) or in the Balearic Islands (western Mediterranean Sea), showed a
570 general decreasing trend for the last ~2000 years, with a warm MCA, a cold LIA, and
571 cold/moderate temperatures for the Industrial Period that do not appear to mirror the
572 modern global warming observed throughout the 20th century ([Abrantes et al., 2005](#);
573 [Moreno et al., 2012](#)). Only high-resolution U^K₃₇-and TEX₈₆-derived (from GDGTs) SST
574 records of the cores 384B and 436B from the Alboran Sea ([Nieto-Moreno et al., 2013](#))
575 and the U^K₃₇-SST record of core Gol-Ho1B from the Gulf of Lion ([Sicre et al., 2016](#))
576 have shown a clear temperature increase during the 20th century, similar to the LDI
577 temperature record in LdRS ([Fig. 5a,d, 6a,c](#)). The observed heterogeneity in the SST
578 reconstructions based on different biomarkers such as alkenones ([Abrantes et al., 2005](#);
579 [Moreno et al., 2012](#); [Rodrigo-Gámiz et al., 2014](#)), GDGTs ([Nieto-Moreno et al., 2013](#)) or
580 LCDs ([Rodrigo-Gámiz et al., 2014](#)) could be explained since each record belongs to a
581 different biogeographical area influenced by specific temporal and dynamic
582 oceanographic regimes, as well as by different primary productivity patterns of each
583 biological source (e.g., seasonality or bloom length) ([Sicre et al., 2016](#)).

584

585 The previously described climate variability in precipitation and temperature
586 during the last ~1500 years in the Iberian Peninsula have been explained by different
587 forcing mechanisms such as the effect of the westerlies-North Atlantic climate dynamics,
588 internal climate variability, solar irradiance, volcanism, or anthropogenic forcing
589 ([Gómez-Navarro et al., 2011](#); [Gómez-Navarro et al., 2012](#); [Moreno et al., 2012](#); [Sánchez-](#)
590 [López et al., 2016](#)). Their potential effect on the **LCD distribution in the** LdRS records is
591 discussed in the following section.

592

593 **4.3. Control mechanisms on alpine temperatures in SW Europe during the**

594 **Common Era**

595

596 This discussion is based on the LDI-temperature reconstruction. However, similar
597 results are obtained when comparing the temperature reconstructions from MLR
598 calibrations 1, 2, and 3 in LdRS and the different forcing mechanisms assessed in this
599 section (Tables S10-S13).

600

601 Solar, volcanic, and anthropogenic (e.g., CO₂ and CH₄) radiative changes, along
602 with the internal variability are usually attributed as the leading factors controlling
603 temperatures during the Common Era ([Ammann et al., 2007](#); [IPCC, 2013](#)). In addition,
604 North Atlantic climate dynamics such as the North Atlantic Oscillation (NAO) or the
605 Atlantic Multidecadal Oscillation (AMO) are other potential drivers of natural climate
606 variability in the Iberian Peninsula ([López-Moreno et al., 2011](#); [Moreno et al., 2012](#);
607 [O'Reilly et al., 2017](#); [Sánchez-López et al., 2016](#)). The control of the North Atlantic
608 climate dynamics in the studied alpine wetlands is evident, at least for precipitation and
609 humidity fluctuations, since the NAO and solar forcing have been described as the main
610 controls on the paleoenvironmental evolution recorded in this area ([Garcia-Alix et al.,](#)
611 [2017](#); [Ramos-Román et al., 2016](#)). Conversely, other studies have shown that the NAO
612 climate mode had little effect on temperatures in this alpine area from 1950 to 2006 CE
613 ([López-Moreno et al., 2011](#)). LdRS data agree with this observation, since no correlation
614 (Tables S10-S13) has been detected between the NAO reconstruction ([Trouet et al., 2009](#))
615 and the obtained LCD record for the last millennium. The AMO has an impact on the
616 North Atlantic atmospheric blocking mechanisms ([Häkkinen et al., 2011](#)) and on the
617 European and Mediterranean temperatures, especially during the AMO warm phases

618 (O'Reilly et al., 2017). In the study area, the AMO shows a moderate long-term
619 correlation (Figs. 5d,e and 6c,d $r>0.60$; $p<0.01$) with both long and short core derived-
620 LDI records, but the correlation decreases when long-term trends are removed ($r<0.32$;
621 $p>0.1$) (Tables S10, S11). Since the nature of the AMO and its specific drivers are still
622 a matter of debate, i.e., internal ocean variability control (multidecadal fluctuations in
623 the Atlantic Meridional Overturning Circulation) versus solar or volcanic forcing for
624 the last centuries ([Knudsen et al., 2014](#)), we cannot conclude whether the observed
625 correlations represent the sole effect of the AMO or the influence of its underlying
626 forcing mechanisms.

627

628 The significant correlation at long and short terms ($r>0.61$; $p<0.005$) between
629 LDI-derived temperatures from LdRS records and greenhouse gases (Schmidt et al.,
630 2011) ([Fig. 6c, g](#); Table S10), especially since the beginning of the 20th century (Industrial
631 Period) ([Fig. 5d,g](#); Table S11), suggests that greenhouse gases might have an important
632 effect on temperatures at this high elevation site.

633

634 The potential impact of solar radiation and volcanic eruptions on climate over both
635 short- and long-time scales is a topic of controversy in the literature ([Ammann et al.,
636 2007](#)). In this regard, volcanic forcing, which should give rise to negative radiative
637 forcing in the climate system ([Ammann et al., 2007](#); [Sigl et al., 2015](#)), do not show a
638 significant correlation with LDI-derived temperatures from LdRS records over the last
639 1500 years ([Figs. 5d,h and 6c,h](#); Table S10, S11). We suggest that this lack of influence
640 at LdRS records is a function of its high-altitude location, at 3020 masl, in the free
641 troposphere, which reduces the environmental impact of small volcanic tropospheric
642 eruptions that likely have greater effects on lower elevation sites ([Mather et al., 2013](#)). In

643 addition, the relatively short residence time of volcanic aerosols in the atmosphere mainly
644 causes, at most, decadal-timescale effects ([Sigl et al., 2015](#)) that can be difficult to identify
645 in most sedimentary records due to the age resolution, as in the case of older sediments
646 than 200 years in LdRS. Nevertheless, large explosive volcanic eruptions delivering large
647 amounts of stratospheric aerosols ([Marotzke and Forster, 2015](#); [Sigl et al., 2015](#)), such as
648 that for Agung Volcano in Bali, Indonesia (1963-1964 CE), may be associated with a
649 small depression in LDI-derived temperatures observed in LdRS records ([Fig. 5d,h](#)).
650 Although cold LDI-reconstructed temperatures occasionally seem to occur coevally with
651 volcanic eruptions, for example, 560-510 and 320 years ago (~1450-1500 and 1690 CE)
652 ([Sigl et al., 2015](#)), there is no consistent relationship between the intensity - number of
653 large eruptions and the reconstructed coolings in LdRS records, especially over the last
654 ~200 years when the age sample resolution would be enough to detect them (LdRS shc).

655
656 Most of the above-mentioned cooling events recorded in LdRS, such as those
657 during the LIA, are coeval with low solar activity periods like the Spörer Minimum (from
658 ~1450 to 1550 CE) or the Maunder Minimum (from ~1645 to 1715 CE) ([Stuiver and](#)
659 [Quay, 1980](#)) ([Fig. 6](#)). Thus, long-term correlations between LDI-derived temperatures
660 and solar activity, based on reconstructions of the solar irradiance and cosmogenic
661 isotopes (such as ^{14}C), are evident during the last ~1500 years in LdRS record ($r>0.69$; p
662 <0.002) ([Fig. 6c,e,f](#); Table S11). This correlation drops ($0.37 < r < 0.56$ and $0.04 < p < 0.14$)
663 when long-term trends are removed (Table S11). The long-term solar influence agrees
664 with previous observations in other alpine records of this area ([Garcia-Alix et al., 2017](#);
665 [Ramos-Román et al., 2016](#)). Solar activity slightly decreases its long-term influence in
666 LdRS record during the last ~200 years ($r>0.56$; $p<0.001$) and disappears when long-term
667 trends are removed (Table S10). Only some occasional temperature decreases or slower

668 rates of warming such as during the 19th to 20th century transition, from ~1930 to 1940,
669 from ~1960 to 1975, and around 1988 CE, **are coeval** with slight declines in the total solar
670 activity (**Fig. 5d,f**: blue arrows).

671

672 In the same way, LdRS registered a small decrease in LDI-derived temperatures
673 (or stabilization) at the beginning of the 21st century (**Fig. 5d**), also recorded in the Madrid
674 and Sevilla temperature time-series ([Spanish National Weather Agency - AEMet Open
675 Data, 2019](#)), **and thus in the reconstructed reference temperatures time-series at 3020 masl**
676 **(Fig. 5c)**, in tree ring records of the the Pyrenees and Iberian Range ([Büntgen et al., 2017](#);
677 [Tejedor et al., 2017](#)), in marine platforms of the western Mediterranean (**Fig. 5a**) ([Sicre
678 et al., 2016](#)), **and globally** ([Fyfe et al., 2016](#)). Although this slowdown agrees with a
679 decreasing trend in solar activity and a slight stabilization of atmospheric methane
680 concentrations (**Fig. 5f,g**), the causes are more complex, and probably related to a
681 combination of internal variability and radiative forcing (e.g., volcanic and solar
682 activity, or decadal timescale changes in anthropogenic aerosols) ([Fyfe et al., 2016](#)).

683

684 **4.4. Exceeding natural thresholds in alpine areas**

685

686 The LDI-derived temperatures from LdRS **exceeded the highest pre-industrial**
687 **temperatures in the early 1950s** (**Fig. 6c**), under full anthropogenic influence. The
688 comparison between pre-industrial and post-industrial scenarios in the study site
689 highlights the human impact on natural trends. **In this regard**, the temperature increase
690 during the last stages of the LIA (from ~1690 to ~1850 CE), an analogue for a non-
691 anthropogenic temperature-increase scenario, was **between ~1.2 and ~1.4°C**
692 **(~0.09°C/decade; Fig. 6)**, whereas the mean temperature rise throughout the 20th century

693 was $\sim 1.8^{\circ}\text{C}$ ($\sim 0.18^{\circ}\text{C}/\text{decade}$; Fig. 7). Both warming rates are roughly similar to those
694 reconstructed from MLR calibrations 1, 2, and 3: $\sim 0.06\text{-}0.09^{\circ}\text{C}/\text{decade}$ for the last stages
695 of the LIA, and $\sim 0.17\text{-}0.18^{\circ}\text{C}/\text{decade}$ for the 20th century. Although this means that on
696 average, the warming rate was two times faster throughout the 20th century than at the
697 end of the LIA (Fig. 7), these observations are based on a low sample density for the LIA
698 (8 samples), which might slightly increase the uncertainty for this period. By comparison,
699 average global temperatures rose by $\sim 0.85^{\circ}\text{C}$ from 1880 to 2012 CE, corresponding to
700 $0.06^{\circ}\text{C}/\text{decade}$ (IPCC, 2013), which highlight the high-elevation amplification effect of
701 temperatures on this vulnerable area.

702

703 Other European alpine areas in the Mediterranean region, such as those from the
704 Alps, experienced a slower warming rate during the 20th century ($\sim 0.11^{\circ}\text{C}/\text{decade}$) (Fig.
705 7) (Auer et al., 2007; Böhm et al., 2010). This is ~ 1.6 times slower than the warming rate
706 recorded in the Sierra Nevada. This evidence, along with the generally smaller amount of
707 precipitation in the alpine areas of the western Mediterranean region (Auer et al., 2007;
708 Rodrigo et al., 1999), allows us to conclude that the 20th century environmental stress in
709 this area was greater than in the Alps.

710

711 Future scenarios are not optimistic for Sierra Nevada since temperatures at ~ 1000
712 masl may rise between 2.2°C and 5.3°C by the end of the 21st century (Pérez-Luque et al.,
713 2016), exceeding the global projections of the IPCC-2013 report (IPCC, 2013). However,
714 temperature projection and its subsequent impact on alpine areas of the Sierra Nevada
715 have not been satisfactorily assessed so far due to the lack of long-term quantitative
716 climatic records at these elevations (e.g., temperature). The LCD-based temperatures at
717 ~ 3000 masl will solve this lack of quantitative data and will be valuable to project future

718 scenarios in these alpine ecosystems where endemic and endangered species inhabit
719 ([Blanca, 2001](#); [Munguira and Martin, 1993](#)).

720

721 **4.5. Impact on the southwesternmost European alpine glaciers**

722

723 The studied alpine area supported the southernmost glaciers in Europe during the
724 LIA. Glaciers and permanent snow fields below ~3000 masl, such as those of Corral del
725 Mulhacen (~2950 masl) whose last mention in the literature was between 1809 and 1849
726 CE ([Oliva and Gomez-Ortiz, 2012](#)), would have totally disappeared by the decrease in
727 regional precipitation during the first half of the 19th century ([Rodrigo et al., 1999](#)). The
728 climatic features at the end of the 19th century and the beginning of the 20th century did
729 not allow this glacier to re-establish itself (Fig. 8). Post-LIA climatic conditions have also
730 been proposed as the trigger for the melting of the Corral del Veleta Glacier in Sierra
731 Nevada (~3100 masl) at the beginning of the 20th century ([Garcia-Alix et al., 2017](#); [Oliva
732 and Gomez-Ortiz, 2012](#); [Oliva et al., 2018](#)). However, the LCDs in LdRS records show
733 that derived-temperatures did not exceed the levels of the 1850s until the late 1940s CE.
734 Precipitation was low in the southern Iberian Peninsula during the first half of the 20th
735 century, but similar, and even lower, precipitation values were registered before ~1850
736 CE ([Rodrigo et al., 1999](#); [Spanish National Weather Agency - AEMet Open Data, 2019](#))
737 (Fig. 8). Therefore, how could the glacier have retreated under this almost steady-state
738 scenario? A similar paradox has been described in the Alps ([Painter et al., 2013](#)), where
739 glaciers began to sharply retreat after the mid-19th century, even though temperature and
740 precipitation records would suggest that glacier expansion should have occurred at least
741 until the first decades of the 20th century. In this case, one of the proposed triggers for the
742 glacier retreat was the industrial black carbon deposition that amplified the solar radiation

743 absorbed at the snow surface and caused its subsequent melting - not a temperature or
744 precipitation change ([Painter et al., 2013](#)). [Precipitation data from the southern Iberia](#)
745 [\(Rodrigo et al., 1999\)](#) along with the LCD-reconstructed temperatures in LdRS records
746 suggest that temperature and precipitation were not the only drivers of glacial retreat that
747 led to the melting of permanent glaciers in the Sierra Nevada in the 1920s. Instead,
748 mirroring the case of the Alps, it is plausible that other factors reducing the albedo, such
749 as enhanced atmospheric deposition may have played a strong role. In this regard,
750 important atmospheric depositional events have been recorded in the study alpine sites of
751 southern Iberia from the mid-19th century to the first decades of the 20th century caused
752 by both enhanced North African dust fluxes ([Mulitza et al., 2010](#)) ([Jiménez et al., 2018](#))
753 as well as a spike in atmospheric pollution (as observed in anthropogenic Pb and Hg
754 records in Sierra Nevada; Fig. 8) ([Garcia-Alix et al., 2017](#); [Garcia-Alix et al., 2013](#)).
755 Similarly, both phenomena have been demonstrated as triggers for glacier retreat ([Painter](#)
756 [et al., 2013](#)) and snow melt in the Alps ([Di Mauro et al., 2018](#)).

757

758 Melting of the last glaciated area in the Sierra Nevada during the first decades of
759 the 20st century ([Grunewald and Scheithauer, 2010](#)) represents an important turning point
760 regarding recent environmental change in this alpine region ([Garcia-Alix et al., 2017](#);
761 [Jiménez et al., 2019](#)). The rapid pace of environmental change in the area after this date
762 is attributed to an amplified effect of warming and aridification (Fig. 8b,c) that increased
763 stress on vulnerable ecosystems ([Garcia-Alix et al., 2017](#); [Jiménez et al., 2019](#); [Jiménez](#)
764 [et al., 2018](#)) with little hope for return of local glaciers.

765

766 **5. Concluding remarks**

767

768 This study shows the vulnerability of alpine regions and the importance of their
769 monitoring for a better understanding of climate variability and future rapid responses. In
770 this regard, algal-derived biomarkers from LdRS records have given rise to the first long-
771 chain **alky** diol temperature calibration in freshwater environments by means of the
772 comparison with instrumental **temperature time-series**. The combination of **both** short and
773 long sediment cores has provided both a highly accurate **LCD**-temperature calibration for
774 the instrumental period and a long-term historical perspective on the modern warming.
775 This approach delivers a better time-integrated temperature model than discrete
776 temperature measurements for the 20th century. **Nevertheless, the lack of information**
777 **about the biological sources of LCDs in the Sierra Nevada means that this calibration can**
778 **only be potentially applied to other lakes with a similar LCD distribution or in the same**
779 **alpine area.**

780
781 The low sample resolution in the longer core before ~1500 CE precludes us from
782 **totally constraining** the main natural controls on temperatures in this high-elevation site
783 for the Common Era. However, the general trends support that the presumed primary
784 effect of greenhouse gases on temperatures reconstructed from algal-lipids in this alpine
785 region of southern Iberia is likely modulated by long-term solar forcing. In recent times,
786 greenhouse gases seem to be the major temperature driver in this high elevation site.
787 Volcanic forcing appears to have little effect on reconstructed temperatures in this alpine
788 area. The Atlantic Multidecadal Oscillation (AMO) have also shown to have a long-term
789 effect in the study area; however, due its complex nature, the real effect of the AMO on
790 **LCD**-reconstructed temperatures in LdRS **records** cannot be fully constrained. In any
791 case, the effect of the internal climate variability on local temperatures cannot be ruled
792 out. LdRS records also highlight the potential impact that non-climatic environmental

793 drivers such as atmospheric dust and pollution deposition can have exerted on these
794 remote alpine environments (e.g., glacier melting).

795

796 Alpine temperatures of southern Iberia exceeded the highest scores reached during
797 pre-industrial times in the 1950s. This means that the rate of warming throughout the 20th
798 century doubled that of the last stages of the LIA. Furthermore, this modern warming rate
799 is even higher in the Sierra Nevada than in the Alps, pointing towards more environmental
800 stress in the Sierra Nevada ecosystems. In addition to the amplified effect of warming
801 and aridification, the local environmental pressure may have enhanced throughout the
802 20th century due to the disappearance of perennial snow fields and the gradual reduction
803 of the seasonal snow cover affecting the local water availability. This fragile alpine
804 environment will suffer severe consequences if the warming rates continue to be so high
805 or even higher as predicted by the end of the 21st century.

806

807 **Data availability.** Fractional abundances of the C₂₈ 1,13-diol, C₂₈ 1,14-diol, C₃₀ 1,13-
808 diol, C₃₀ 1,14-diol, C₃₀ 1,15-diol, and C₃₂ 1,15-diol from the studied cores (LdRS shc and
809 LdRS lgc) are available in Table S14, along with the four reference temperature time-
810 series at 3020 masl from 1908 to 2008.

811

812 **Supplement.** The supplement related to this article is available online at:

813 <https://doi.org/>

814

815 **Author contributions.** The study was conceived by AG-A and JLT. CPM, LJ, GJM,
816 and RSA recovered the sediment cores. AG-A analysed the samples and processed the

817 data. All co-authors discussed the data and equally contributed to the preparation of the
818 manuscript.

819

820 **Competing interests.** The authors declare that they have no conflict of interest.

821

822 **Acknowledgements.** We would like to thank to V. Slaymark (University of Glasgow),
823 for her help preparing and analysing the organic and inorganic samples, as well as F.J.
824 Bonet García, C. González Hidalgo, and M.J. Esteban Parra for providing the temperature
825 time-series from Sierra Nevada and South of Spain.

826

827 **Financial support.** This study was supported by the project P11-RNM 7332 of the “Junta
828 de Andalucía”, the projects CGL2017-85415-R, CGL2013-47038-R and CGL2011-
829 23483 of the “Ministerio de Economía y Competitividad of Spain and Fondo Europeo de
830 Desarrollo Regional FEDER”, the project 87/2007 of the OAPN-Ministerio de Medio
831 Ambiente, as well as the research group RNM-190 (Junta de Andalucía). A.G.-A. was
832 also supported by a Marie Curie Intra-European Fellowship of the 7th Framework
833 Programme for Research, Technological Development and Demonstration of the
834 European Commission (NAOSIPUK. Grant Number: PIEF-GA-2012-623027) and by a
835 Ramón y Cajal Fellowship RYC-2015-18966 of the Spanish Government (Ministerio de
836 Economía y Competitividad). J.L.T. hosted the NAOSIPUK project (PIEF-GA-2012-
837 623027) at the University of Glasgow.

838

839 **References**

840

841 Abrantes, F., Lebreiro, S., Rodrigues, T., Gil, I., Bartels-Jónsdóttir, H., Oliveira, P.,
842 Kissel, C., and Grimalt, J. O.: Shallow-marine sediment cores record climate

843 variability and earthquake activity off Lisbon (Portugal) for the last 2000 years,
844 Quaternary Science Reviews, 24, 2477-2494, 2005.

845 Ammann, C. M., Joos, F., Schimel, D. S., Otto-Bliesner, B. L., and Tomas, R. A.: Solar
846 influence on climate during the past millennium: Results from transient
847 simulations with the NCAR Climate System Model, Proceedings of the National
848 Academy of Sciences, 104, 3713-3718, 2007.

849 Anderson, R. S., Jiménez-Moreno, G., Carrión, J., and Pérez-Martinez, C.: Postglacial
850 history of alpine vegetation, fire, and climate from Laguna de Río Seco, Sierra
851 Nevada, southern Spain, Quaternary Science Reviews, 30, 1615–1629, 2011.

852 Auer, I., Böhm, R., Jurkovic, A., Lipa, W., Orlik, A., Potzmann, R., Schöner, W.,
853 Ungersböck, M., Matulla, C., Briffa, K., Jones, P., Efthymiadis, D., Brunetti, M.,
854 Nanni, T., Maugeri, M., Mercalli, L., Mestre, O., Moisselin, J.-M., Begert, M.,
855 Müller-Westermeier, G., Kveton, V., Bochnicek, O., Stastny, P., Lapin, M.,
856 Szalai, S., Szentimrey, T., Cegnar, T., Dolinar, M., Gajic-Capka, M., Zaninovic,
857 K., Majstorovic, Z., and Nieplova, E.: HISTALP—historical instrumental
858 climatological surface time series of the Greater Alpine Region, International
859 Journal of Climatology, 27, 17-46, 2007.

860 Balzano, S., Lattaud, J., Villanueva, L., Rampen, S. W., Brussaard, C. P. D., van
861 Bleijswijk, J., Bale, N., Sinninghe Damsté, J. S., and Schouten, S.: A quest for the
862 biological sources of long chain alkyl diols in the western tropical North Atlantic
863 Ocean, Biogeosciences, 15, 5951-5968, 2018.

864 Barea-Arco, J., Pérez-Martínez, C., and Morales-Baquero, R.: Evidence of a mutualistic
865 relationship between an algal epibiont and its host, *Daphnia pulicaria*, Limnology
866 and Oceanography, 46, 871-881, 2001.

867 Blanca, G.: Flora amenazada y endémica de Sierra Nevada, Consejería de Medio
868 Ambiente de la Junta de Andalucía and University of Granada, 2001.

869 Böhm, R., Jones, P. D., Hiebl, J., Frank, D., Brunetti, M., and Maugeri, M.: The early
870 instrumental warm-bias: a solution for long central European temperature series
871 1760–2007, Climatic Change, 101, 41-67, 2010.

872 Büntgen, U., Krusic, P. J., Verstege, A., Sangüesa-Barreda, G., Wagner, S., Camarero,
873 J. J., Ljungqvist, F. C., Zorita, E., Oppenheimer, C., Konter, O., Tegel, W.,
874 Gärtner, H., Cherubini, P., Reinig, F., and Esper, J.: New Tree-Ring Evidence
875 from the Pyrenees Reveals Western Mediterranean Climate Variability since
876 Medieval Times, Journal of Climate, 30, 5295-5318, 2017.

877 Carrillo, P., Cruz-Pizarro, L., and Sánchez Castillo, P. M.: Aportación al conocimiento
878 del ciclo biológico de *Chromulina nevadensis*, *Acta Botánica Malacitana*, 16, 19-
879 26, 1991.

880 Castañeda, I. S. and Schouten, S.: A review of molecular organic proxies for examining
881 modern and ancient lacustrine environments, *Quaternary Science Reviews*, 30,
882 2851-2891, 2011.

883 Castillo Martín, A.: *Lagunas de Sierra Nevada*, Editorial Universidad de Granada,
884 Granada, 2009.

885 Catalan, J., Pla-Rabés, S., Wolfe, A. P., Smol, J. P., Rühland, K. M., Anderson, N. J.,
886 Kopáček, J., Stuchlík, E., Schmidt, R., Koinig, K. A., Camarero, L., Flower, R. J.,
887 Heiri, O., Kamenik, C., Korhola, A., Leavitt, P. R., Psenner, R., and Renberg, I.:
888 Global change revealed by palaeolimnological records from remote lakes: a
889 review, *Journal of Paleolimnology*, 49, 513-535, 2013.

890 Coddington, O., Lean, J. L., Pilewskie, P., Snow, M., and Lindholm, D.: A Solar
891 Irradiance Climate Data Record, *Bulletin of the American Meteorological*
892 *Society*, 97, 1265-1282, 2016.

893 Colcord, D. E., Cadieux, S. B., Brassell, S. C., Castañeda, I. S., Pratt, L. M., and White,
894 J. R.: Assessment of branched GDGTs as temperature proxies in sedimentary
895 records from several small lakes in southwestern Greenland, *Organic*
896 *Geochemistry*, 82, 33-41, 2015.

897 de Bar, M. W., Dorhout, D. J. C., Hopmans, E. C., Rampen, S. W., Sinninghe Damsté,
898 J. S., and Schouten, S.: Constraints on the application of long chain diol proxies in
899 the Iberian Atlantic margin, *Organic Geochemistry*, 101, 184-195, 2016.

900 Di Mauro, B., Garzonio, R., Rossini, M., Filippa, G., Pogliotti, P., Galvagno, M., Morra
901 di Cella, U., Migliavacca, M., Baccolo, G., Clemenza, M., Delmonte, B., Maggi,
902 V., Dumont, M., Tuzet, F., Lafaysse, M., Morin, S., Cremonese, E., and Colombo,
903 R.: Saharan dust events in the European Alps: role on snowmelt and geochemical
904 characterization, *The Cryosphere Discuss.*, 2018, 1-28, 2018.

905 Easterling, D. R., Meehl, G. A., Parmesan, C., Changnon, S. A., Karl, T. R., and
906 Mearns, L. O.: Climate Extremes: Observations, Modeling, and Impacts, *Science*,
907 289, 2068-2074, 2000.

908 Foster, L. C., Pearson, E. J., Juggins, S., Hodgson, D. A., Saunders, K. M., Verleyen,
909 E., and Roberts, S. J.: Development of a regional glycerol dialkyl glycerol

910 tetraether (GDGT)–temperature calibration for Antarctic and sub-Antarctic lakes,
911 Earth and Planetary Science Letters, 433, 370-379, 2016.

912 Fyfe, J. C., Meehl, G. A., England, M. H., Mann, M. E., Santer, B. D., Flato, G. M.,
913 Hawkins, E., Gillett, N. P., Xie, S.-P., Kosaka, Y., and Swart, N. C.: Making
914 sense of the early-2000s warming slowdown, Nature Climate Change, 6, 224,
915 2016.

916 Gal, J.-K., Kim, J.-H., and Shin, K.-H.: Distribution of long chain alkyl diols along a
917 south-north transect of the northwestern Pacific region: Insights into a paleo sea
918 surface nutrient proxy, Organic Geochemistry, 119, 80-90, 2018.

919 García Montoro, C., Titos Martínez, M., and Casado Sánchez de Castilla, M.: Sierra
920 Nevada. Una expedición al pico de Veleta desde los Baños de Lanjarón (1859),
921 Universidad de Granada, Editorial Universidad de Granada, 2016.

922 Garcia-Alix, A., Jimenez Espejo, F. J., Toney, J. L., Jiménez-Moreno, G., Ramos-
923 Román, M. J., Anderson, R. S., Ruano, P., Queralt, I., Delgado Huertas, A., and
924 Kuroda, J.: Alpine bogs of southern Spain show human-induced environmental
925 change superimposed on long-term natural variations, Scientific Reports, 7, 7439
926 2017.

927 Garcia-Alix, A., Jimenez-Espejo, F. J., Lozano, J. A., Jimenez-Moreno, G., Martinez-
928 Ruiz, F., Garcia Sanjuan, L., Aranda Jimenez, G., Garcia Alfonso, E., Ruiz-
929 Puertas, G., and Anderson, R. S.: Anthropogenic impact and lead pollution
930 throughout the Holocene in Southern Iberia, Science of the Total Environment,
931 449, 451-460, 2013.

932 García-Alix, A., Jiménez-Moreno, G., Anderson, R. S., Jiménez Espejo, F. J., and
933 Delgado Huertas, A.: Holocene environmental change in southern Spain deduced
934 from the isotopic record of a high-elevation wetland in Sierra Nevada, Journal of
935 Paleolimnology, 48, 471-484, 2012.

936 Giorgi, F.: Climate change hot-spots, Geophysical Research Letters, 33, 2006.

937 Gómez-Navarro, J. J., Montávez, J. P., Jerez, S., Jiménez-Guerrero, P., Lorente-Plazas,
938 R., González-Rouco, J. F., and Zorita, E.: A regional climate simulation over the
939 Iberian Peninsula for the last millennium, Clim. Past, 7, 451-472, 2011.

940 Gómez-Navarro, J. J., Montávez, J. P., Jiménez-Guerrero, P., Jerez, S., Lorente-Plazas,
941 R., González-Rouco, J. F., and Zorita, E.: Internal and external variability in
942 regional simulations of the Iberian Peninsula climate over the last millennium,
943 Clim. Past, 8, 25-36, 2012.

944 Gonzalez-Hidalgo, J. C., Peña-Angulo, D., Brunetti, M., and Cortesi, N.: MOTEDAS: a
945 new monthly temperature database for mainland Spain and the trend in
946 temperature (1951–2010), *International Journal of Climatology*, 35, 4444-4463,
947 2015.

948 Grunewald, K. and Scheithauer, J.: Europe's southernmost glaciers: response and
949 adaptation to climate change, *Journal of Glaciology*, 56, 129-142, 2010.

950 Häkkinen, S., Rhines, P. B., and Worthen, D. L.: Atmospheric Blocking and Atlantic
951 Multidecadal Ocean Variability, *Science*, 334, 655-659, 2011.

952 Hansen, J., Ruedy, R., Sato, M., and Lo, K.: Global Surface Temperature Change,
953 *Reviews of Geophysics*, 48, 2010.

954 IPCC: Climate Change 2013: The Physical Science Basis. Contribution of Working
955 Group I to the Fifth Assessment Report of the Intergovernmental Panel on
956 Climate Change, Cambridge University Press, Cambridge, United Kingdom and
957 New York, NY, USA, 2013.

958 Jiménez, L., Conde-Porcuna, J. M., García-Alix, A., Toney, J. L., Anderson, R. S.,
959 Heiri, O., and Pérez-Martínez, C.: Ecosystem Responses to Climate-Related
960 Changes in a Mediterranean Alpine Environment Over the Last ~ 180 Years,
961 *Ecosystems*, 22, 563-577, 2019.

962 Jiménez, L., Romero-Viana, L., Conde-Porcuna, J. M., and Pérez-Martínez, C.:
963 Sedimentary photosynthetic pigments as indicators of climate and watershed
964 perturbations in an alpine lake in southern Spain, *Limnologia*, 34, 439-454, 2015.

965 Jiménez, L., Rühland, K. M., Jeziorski, A., Smol, J. P., and Pérez-Martínez, C.: Climate
966 change and Saharan dust drive recent cladoceran and primary production changes
967 in remote alpine lakes of Sierra Nevada, Spain, *Global Change Biology*, 28,
968 e139–e158, 2018.

969 Jiménez-Espejo, F. J., García-Alix, A., Jiménez-Moreno, G., Rodrigo-Gámiz, M.,
970 Anderson, R. S., Rodríguez-Tovar, F. J., Martínez-Ruiz, F., Giralt, S., Delgado
971 Huertas, A., and Pardo-Igúzquiza, E.: Saharan aeolian input and effective
972 humidity variations over western Europe during the Holocene from a high altitude
973 record, *Chemical Geology*, 374-375, 1-12, 2014.

974 Jiménez-Moreno, G. and Anderson, R. S.: Holocene vegetation and climate change
975 recorded in alpine bog sediments from the Borreguiles de la Virgen, Sierra
976 Nevada, southern Spain, *Quaternary Research*, 77, 44-53, 2012.

977 Jiménez-Moreno, G., García-Alix, A., Hernández-Corbalán, M. D., Anderson, R. S.,
978 and Delgado-Huertas, A.: Vegetation, fire, climate and human disturbance history
979 in the southwestern Mediterranean area during the late Holocene, *Quaternary*
980 *Research*, 79, 110-122, 2013.

981 Knudsen, M. F., Jacobsen, B. H., Seidenkrantz, M.-S., and Olsen, J.: Evidence for
982 external forcing of the Atlantic Multidecadal Oscillation since termination of the
983 Little Ice Age, *Nature Communications*, 5, 3323, 2014.

984 Lattaud, J., Dorhout, D., Schulz, H., Castañeda, I. S., Schefuß, E., Sinninghe Damsté, J.
985 S., and Schouten, S.: The C32 alkane-1,15-diol as a proxy of late Quaternary
986 riverine input in coastal margins, *Clim. Past*, 13, 1049-1061, 2017a.

987 Lattaud, J., Kim, J.-H., De Jonge, C., Zell, C., Sinninghe Damsté, J. S., and Schouten,
988 S.: The C32 alkane-1,15-diol as a tracer for riverine input in coastal seas,
989 *Geochimica et Cosmochimica Acta*, 202, 146-158, 2017b.

990 Lattaud, J., Kirkels, F., Peterse, F., Freymond, C. V., Eglinton, T. I., Hefter, J.,
991 Mollenhauer, G., Balzano, S., Villanueva, L., van der Meer, M. T. J., Hopmans,
992 E. C., Sinninghe Damsté, J. S., and Schouten, S.: Long-chain diols in rivers:
993 distribution and potential biological sources, *Biogeosciences*, 15, 4147-4161,
994 2018a.

995 Lattaud, J., Lo, L., Huang, J.-J., Chou, Y.-M., Gorbarenko, S. A., Sinninghe Damsté, J.
996 S., and Schouten, S.: A Comparison of Late Quaternary Organic Proxy-Based
997 Paleotemperature Records of the Central Sea of Okhotsk, *Paleoceanography and*
998 *Paleoclimatology*, 33, 732-744, 2018b.

999 Longo, W. M., Huang, Y., Yao, Y., Zhao, J., Giblin, A. E., Wang, X., Zech, R.,
1000 Haberzettl, T., Jardillier, L., Toney, J., Liu, Z., Krivonogov, S., Kolpakova, M.,
1001 Chu, G., D'Andrea, W. J., Harada, N., Nagashima, K., Sato, M., Yonenobu, H.,
1002 Yamada, K., Gotanda, K., and Shinozuka, Y.: Widespread occurrence of distinct
1003 alkenones from Group I haptophytes in freshwater lakes: Implications for
1004 paleotemperature and paleoenvironmental reconstructions, *Earth and Planetary*
1005 *Science Letters*, 492, 239-250, 2018.

1006 López-Moreno, J. I., Vicente-Serrano, S. M., Morán-Tejeda, E., Lorenzo-Lacruz, J.,
1007 Kenawy, A., and Beniston, M.: Effects of the North Atlantic Oscillation (NAO)
1008 on combined temperature and precipitation winter modes in the Mediterranean
1009 mountains: Observed relationships and projections for the 21st century, *Global*
1010 *and Planetary Change*, 77, 62-76, 2011.

1011 Luterbacher, J., Werner, J. P., Smerdon, J. E., Fernández-Donado, L., González-Rouco,
 1012 F. J., Barriopedro, D., Ljungqvist, F. C., Büntgen, U., Zorita, E., Wagner, S.,
 1013 Esper, J., McCarroll, D., Toreti, A., Frank, D., Jungclaus, J. H., Barriendos, M.,
 1014 Bertolin, C., Bothe, O., Brázdil, R., Camuffo, D., Dobrovolný, P., Gagen, M.,
 1015 García-Bustamante, E., Ge, Q., Gómez-Navarro, J. J., Guiot, J., Hao, Z., Hegerl,
 1016 G. C., Holmgren, K., Klimenko, V. V., Martín-Chivelet, J., Pfister, C., Roberts,
 1017 N., Schindler, A., Schurer, A., Solomina, O., von Gunten, L., Wahl, E., Wanner,
 1018 H., Wetter, O., Xoplaki, E., Yuan, N., Zanchettin, D., Zhang, H., and Zerefos, C.:
 1019 European summer temperatures since Roman times, *Environmental Research*
 1020 *Letters*, 11, 024001, 2016.

1021 Mann, M. E., Zhang, Z., Rutherford, S., Bradley, R. S., Hughes, M. K., Shindell, D.,
 1022 Ammann, C., Faluvegi, G., and Ni, F.: Global Signatures and Dynamical Origins
 1023 of the Little Ice Age and Medieval Climate Anomaly, *Science*, 326, 1256-1260,
 1024 2009.

1025 Marotzke, J. and Forster, P. M.: Forcing, feedback and internal variability in global
 1026 temperature trends, *Nature*, 517, 565-570, 2015.

1027 Mather, T. A., Pyle, D. M., and Oppenheimer, C.: Tropospheric Volcanic Aerosol. In:
 1028 *Volcanism and the Earth's Atmosphere*, American Geophysical Union, 2013.

1029 Médail, F. and Quézel, P.: Biodiversity Hotspots in the Mediterranean Basin: Setting
 1030 Global Conservation Priorities, *Conservation Biology*, 13, 1510-1513, 1999.

1031 Mesa-Fernández, J. M., Jiménez-Moreno, G., Rodrigo-Gámiz, M., García-Alix, A.,
 1032 Jiménez-Espejo, F. J., Martínez-Ruiz, F., Anderson, R. S., Camuera, J., and
 1033 Ramos-Román, M. J.: Vegetation and geochemical responses to Holocene rapid
 1034 climate change in the Sierra Nevada (southeastern Iberia): the Laguna Hondera
 1035 record, *Clim. Past*, 14, 1687-1706, 2018.

1036 Morales-Baquero, R., Pulido-Villena, E., and Reche, I.: Atmospheric inputs of
 1037 phosphorus and nitrogen to the southwest Mediterranean region: Biogeochemical
 1038 responses of high mountain lakes, *Limnology and Oceanography* 51, 830–837,
 1039 2006.

1040 Moreno, A., Pérez, A., Frigola, J., Nieto-Moreno, V., Rodrigo-Gámiz, M., Martrat, B.,
 1041 González-Sampériz, P., Morellón, M., Martín-Puertas, C., Corella, J. P.,
 1042 Belmonte, Á., Sancho, C., Cacho, I., Herrera, G., Canals, M., Grimalt, J. O.,
 1043 Jiménez-Espejo, F., Martínez-Ruiz, F., Vegas-Vilarrúbia, T., and Valero-Garcés,

1044 B. L.: The Medieval Climate Anomaly in the Iberian Peninsula reconstructed
1045 from marine and lake records, *Quaternary Science Reviews*, 43, 16-32, 2012.

1046 Mulitza, S., Heslop, D., Pittauerova, D., Fischer, H. W., Meyer, I., Stuut, J.-B., Zabel,
1047 M., Mollenhauer, G., Collins, J. A., Kuhnert, H., and Schulz, M.: Increase in
1048 African dust flux at the onset of commercial agriculture in the Sahel region,
1049 *Nature*, 466, 226-228, 2010.

1050 Munguira, M. L. and Martin, J.: The Sierra Nevada blue, *Polyommatus golgus*
1051 (Hiibner). In: *Conservation Biology of Lycaenidae (Butterflies)*, New, T. R. (Ed.),
1052 IUCN, Gland, Switzerland, 1993.

1053 Nieto-Moreno, V., Martínez-Ruiz, F., Willmott, V., García-Orellana, J., Masqué, P., and
1054 Sinninghe Damsté, J. S.: Climate conditions in the westernmost Mediterranean
1055 over the last two millennia: An integrated biomarker approach, *Organic*
1056 *Geochemistry*, 55, 1-10, 2013.

1057 O'Reilly, C. H., Woollings, T., and Zanna, L.: The Dynamical Influence of the Atlantic
1058 Multidecadal Oscillation on Continental Climate, *Journal of Climate*, 30, 7213-
1059 7230, 2017.

1060 Observatorio del cambio global de Sierra Nevada: *Linaria v1.0*. iEcolab – Laboratorio
1061 de Ecología Terrestre – Universidad de Granada, <http://linaria.obsnev.es>, 2016.

1062 Oliva, M. and Gomez-Ortiz, A.: Late-Holocene environmental dynamics and climate
1063 variability in a Mediterranean high mountain environment (Sierra Nevada, Spain)
1064 inferred from lake sediments and historical sources, *The Holocene*, 22, 915-927,
1065 2012.

1066 Oliva, M., Ruiz-Fernández, J., Barriendos, M., Benito, G., Cuadrat, J. M., Domínguez-
1067 Castro, F., García-Ruiz, J. M., Giralt, S., Gómez-Ortiz, A., Hernández, A., López-
1068 Costas, O., López-Moreno, J. I., López-Sáez, J. A., Martínez-Cortizas, A.,
1069 Moreno, A., Prohom, M., Saz, M. A., Serrano, E., Tejedor, E., Trigo, R., Valero-
1070 Garcés, B., and Vicente-Serrano, S. M.: The Little Ice Age in Iberian mountains,
1071 *Earth-Science Reviews*, 177, 175-208, 2018.

1072 Painter, T. H., Flanner, M. G., Kaser, G., Marzeion, B., VanCuren, R. A., and Abdalati,
1073 W.: End of the Little Ice Age in the Alps forced by industrial black carbon,
1074 *Proceedings of the National Academy of Sciences*, 110, 15216-15221, 2013.

1075 Pauli, H., Gottfried, M., Dullinger, S., Abdaladze, O., Akhalkatsi, M., Alonso, J. L. B.,
1076 Coldea, G., Dick, J., Erschbamer, B., Calzado, R. F., Ghosn, D., Holten, J. I.,
1077 Kanka, R., Kazakis, G., Kollár, J., Larsson, P., Moiseev, P., Moiseev, D., Molau,

1078 U., Mesa, J. M., Nagy, L., Pelino, G., Puşcaş, M., Rossi, G., Stanisci, A.,
1079 Syverhuset, A. O., Theurillat, J.-P., Tomaselli, M., Unterluggauer, P., Villar, L.,
1080 Vittoz, P., and Grabherr, G.: Recent Plant Diversity Changes on Europe's
1081 Mountain Summits, *Science*, 336, 353-355, 2012.

1082 Pérez-Luque, A., Pérez-Pérez, R., Aspizua, R., Muñoz, J., and Bonet, F.: Climate in
1083 Sierra Nevada: present and future. . In: Change impacts in Sierra Nevada:
1084 challenges for conservation, Zamora, R., Pérez-Luque, A., Bonet, F., Barea-
1085 Azcón, J., and Aspizua, R. (Eds.), *Consejería de Medio Ambiente y Ordenación
1086 del Territorio, Junta de Andalucía, Andalucía, 2016.*

1087 Pulido-Villena, E., Reche, I., and Morales-Baquero, R.: Food web reliance on
1088 allochthonous carbon in two high mountain lakes with contrasting catchments: a
1089 stable isotope approach, *Canadian Journal of Fisheries and Aquatic Sciences*, 62,
1090 2640–2648 2005.

1091 Ramos-Román, M. J., Jiménez-Moreno, G., R.S., A., García-Alix, A., Toney, J. L.,
1092 Jiménez-Espejo, F. J., and Carrión, J. S.: Centennial-scale vegetation and North
1093 Atlantic Oscillation changes during the Late Holocene in the southern Iberia,
1094 *Quaternary Science Reviews*, 143, 84-95, 2016.

1095 Rampen, S. W., Datema, M., Rodrigo-Gámiz, M., Schouten, S., Reichart, G.-J., and
1096 Sinninghe Damsté, J. S.: Sources and proxy potential of long chain alkyl diols in
1097 lacustrine environments, *Geochimica et Cosmochimica Acta*, 144, 59-71, 2014a.

1098 Rampen, S. W., Schouten, S., Koning, E., Brummer, G.-J. A., and Sinninghe Damsté, J.
1099 S.: A 90 kyr upwelling record from the northwestern Indian Ocean using a novel
1100 long-chain diol index, *Earth and Planetary Science Letters*, 276, 207-213, 2008.

1101 Rampen, S. W., Willmott, V., Kim, J.-H., Rodrigo-Gámiz, M., Uliana, E., Mollenhauer,
1102 G., Schefuß, E., Sinninghe Damsté, J. S., and Schouten, S.: Evaluation of long
1103 chain 1,14-alkyl diols in marine sediments as indicators for upwelling and
1104 temperature, *Organic Geochemistry*, 76, 39-47, 2014b.

1105 Rampen, S. W., Willmott, V., Kim, J.-H., Uliana, E., Mollenhauer, G., Schefuß, E.,
1106 Sinninghe Damsté, J. S., and Schouten, S.: Long chain 1,13- and 1,15-diols as a
1107 potential proxy for palaeotemperature reconstruction, *Geochimica et
1108 Cosmochimica Acta*, 84, 204-216, 2012.

1109 Reche, I., Ortega-Retuerta, E., Romera, O., Pulido-Villena, E., Morales-Baquero, R.,
1110 and Casamayor, E. O.: Effect of Saharan dust inputs on bacterial activity and

- 1111 community composition in Mediterranean lakes and reservoirs, *Limnol.*
1112 *Oceanogr*, 54, 869–879, 2009.
- 1113 Reimer, P. J., Bard, E., Bayliss, A., Beck, J. W., Blackwell, P. G., Ramsey, C. B., Buck,
1114 C. E., Cheng, H., Edwards, R. L., Friedrich, M., Grootes, P. M., Guilderson, T. P.,
1115 Haflidason, H., Hajdas, I., Hatté, C., Heaton, T. J., Hoffmann, D. L., Hogg, A. G.,
1116 Hughen, K. A., Kaiser, K. F., Kromer, B., Manning, S. W., Niu, M., Reimer, R.
1117 W., Richards, D. A., Scott, E. M., Southon, J. R., Staff, R. A., Turney, C. S. M.,
1118 and van der Plicht, J.: IntCal13 and Marine13 Radiocarbon Age Calibration
1119 Curves 0–50,000 Years cal BP, *Radiocarbon*, 55, 1869-1887, 2013.
- 1120 Rodrigo, F. S., Esteban-Parra, M. J., Pozo-Vázquez, D., and Castro-Diez, Y.: A 500-
1121 year precipitation record in Southern Spain, *International Journal of Climatology*,
1122 19, 1233-1253, 1999.
- 1123 Rodrigo-Gámiz, M., Martínez-Ruiz, F., Rampen, S. W., Schouten, S., and Sinninghe
1124 Damsté, J. S.: Sea surface temperature variations in the western Mediterranean
1125 Sea over the last 20 kyr: A dual-organic proxy (UK' 37 and LDI) approach,
1126 *Paleoceanography*, 29, 87-98, 2014.
- 1127 Rodrigo-Gámiz, M., Rampen, S. W., de Haas, H., Baas, M., Schouten, S., and
1128 Sinninghe Damsté, J. S.: Constraints on the applicability of the organic
1129 temperature proxies UK'37, TEX86 and LDI in the subpolar region around
1130 Iceland, *Biogeosciences*, 12, 6573-6590, 2015.
- 1131 Romero-Viana, L., Kienel, U., and Sachse, D.: Lipid biomarker signatures in a
1132 hypersaline lake on Isabel Island (Eastern Pacific) as a proxy for past rainfall
1133 anomaly (1942–2006AD), *Palaeogeography, Palaeoclimatology, Palaeoecology*,
1134 350-352, 49-61, 2012.
- 1135 Sánchez-Castillo, P. M.: Algas de las lagunas de alta montaña de Sierra Nevada
1136 (Granada, España), *Acta Botánica Malacitana*, 13, 21 -52, 1988.
- 1137 Sánchez-López, G., Hernández, A., Pla-Rabes, S., Trigo, R. M., Toro, M., Granados, I.,
1138 Sáez, A., Masqué, P., Pueyo, J. J., Rubio-Inglés, M. J., and Giral, S.: Climate
1139 reconstruction for the last two millennia in central Iberia: The role of East Atlantic
1140 (EA), North Atlantic Oscillation (NAO) and their interplay over the Iberian
1141 Peninsula, *Quaternary Science Reviews*, 149, 135-150, 2016.
- 1142 Schmidt, G. A., Jungclauss, J. H., Ammann, C. M., Bard, E., Braconnot, P., Crowley, T.
1143 J., Delaygue, G., Joos, F., Krivova, N. A., Muscheler, R., Otto-Bliesner, B. L.,
1144 Pongratz, J., Shindell, D. T., Solanki, S. K., Steinhilber, F., and Vieira, L. E. A.:

1145 Climate forcing reconstructions for use in PMIP simulations of the last
1146 millennium (v1.0), *Geosci. Model Dev.*, 4, 33-45, 2011.

1147 Schröter, D., Cramer, W., Leemans, R., Prentice, I. C., Araújo, M. B., Arnell, N. W.,
1148 Bondeau, A., Bugmann, H., Carter, T. R., Gracia, C. A., de la Vega-Leinert, A.
1149 C., Erhard, M., Ewert, F., Glendining, M., House, J. I., Kankaanpää, S., Klein, R.
1150 J. T., Lavorel, S., Lindner, M., Metzger, M. J., Meyer, J., Mitchell, T. D.,
1151 Reginster, I., Rounsevell, M., Sabaté, S., Sitch, S., Smith, B., Smith, J., Smith, P.,
1152 Sykes, M. T., Thonicke, K., Thuiller, W., Tuck, G., Zaehle, S., and Zierl, B.:
1153 Ecosystem Service Supply and Vulnerability to Global Change in Europe,
1154 *Science*, 310, 1333-1337, 2005.

1155 Shimokawara, M., Nishimura, M., Matsuda, T., Akiyama, N., and Kawai, T.: Bound
1156 forms, compositional features, major sources and diagenesis of long chain, alkyl
1157 mid-chain diols in Lake Baikal sediments over the past 28,000 years, *Organic*
1158 *Geochemistry*, 41, 753-766, 2010.

1159 Sicre, M.-A., Jalali, B., Martrat, B., Schmidt, S., Bassetti, M.-A., and Kallel, N.: Sea
1160 surface temperature variability in the North Western Mediterranean Sea (Gulf of
1161 Lion) during the Common Era, *Earth and Planetary Science Letters*, 456, 124-133,
1162 2016.

1163 Sigl, M., Winstrup, M., McConnell, J. R., Welten, K. C., Plunkett, G., Ludlow, F.,
1164 Buntgen, U., Caffee, M., Chellman, N., Dahl-Jensen, D., Fischer, H., Kipfstuhl,
1165 S., Kostick, C., Maselli, O. J., Mekhaldi, F., Mulvaney, R., Muscheler, R.,
1166 Pasteris, D. R., Pilcher, J. R., Salzer, M., Schupbach, S., Steffensen, J. P., Vinther,
1167 B. M., and Woodruff, T. E.: Timing and climate forcing of volcanic eruptions for
1168 the past 2,500 years, *Nature*, 523, 543-549, 2015.

1169 Sinninghe Damsté, J. S., Rampen, S., Irene, W., Rijpstra, C., Abbas, B., Muyzer, G.,
1170 and Schouten, S.: A diatomaceous origin for long-chain diols and mid-chain
1171 hydroxy methyl alkanoates widely occurring in quaternary marine sediments:
1172 indicators for high-nutrient conditions, *Geochimica et Cosmochimica Acta*, 67,
1173 1339-1348, 2003.

1174 Smith, M., De Deckker, P., Rogers, J., Brocks, J., Hope, J., Schmidt, S., Lopes dos
1175 Santos, R., and Schouten, S.: Comparison of U37K', TEX86H and LDI
1176 temperature proxies for reconstruction of south-east Australian ocean
1177 temperatures, *Organic Geochemistry*, 64, 94-104, 2013.

1178 Spanish National Weather Agency - AEMet Open Data: AEMet Open Data.
1179 http://www.aemet.es/es/datos_abiertos/AEMET_OpenData, 2019.

1180 Steinhilber, F., Beer, J., and Fröhlich, C.: Total solar irradiance during the Holocene,
1181 Geophysical Research Letters, 36, 2009.

1182 Stuiver, M. and Quay, P. D.: Changes in Atmospheric Carbon-14 Attributed to a
1183 Variable Sun, Science, 207, 11-19, 1980.

1184 Tejedor, E., Saz, M. Á., Cuadrat, J. M., Esper, J., and de Luis, M.: Temperature
1185 variability in the Iberian Range since 1602 inferred from tree-ring records, Clim.
1186 Past, 13, 93-105, 2017.

1187 Theroux, S., D'Andrea, W. J., Toney, J., Amaral-Zettler, L., and Huang, Y.:
1188 Phylogenetic diversity and evolutionary relatedness of alkenone-producing
1189 haptophyte algae in lakes: Implications for continental paleotemperature
1190 reconstructions, Earth and Planetary Science Letters, 300, 311-320, 2010.

1191 Titos Martínez, M.: Los trabajos de desagüe de las lagunas de Sierra Nevada: un largo
1192 despropósito medioambiental, Revista del Centro de Estudios Históricos de
1193 Granada y su Reino, 2019. 223-243, 2019.

1194 Titos Martínez, M. and Ramos Lafuente, A. J.: El refugio más antiguo de Sierra
1195 Nevada: Construido en 1891, aún se mantiene en pie, Andalucía en la historia,
1196 2016. 48-53, 2016.

1197 Trouet, V., Esper, J., Graham, N. E., Baker, A., Scourse, J. D., and Frank, D. C.:
1198 Persistent Positive North Atlantic Oscillation Mode Dominated the Medieval
1199 Climate Anomaly, Science, 324, 78-80, 2009.

1200 Versteegh, G. J. M., Bosch, H. J., and De Leeuw, J. W.: Potential palaeoenvironmental
1201 information of C24 to C36 mid-chain diols, keto-ols and mid-chain hydroxy fatty
1202 acids; a critical review, Organic Geochemistry, 27, 1-13, 1997.

1203 Villanueva, L., Besseling, M., Rodrigo-Gámiz, M., Rampen, S. W., Verschuren, D., and
1204 Sinninghe Damsté, J. S.: Potential biological sources of long chain alkyl diols in a
1205 lacustrine system, Organic Geochemistry, 68, 27-30, 2014.

1206 Volkman, J. K., Barrett, S. M., and Blackburn, S. I.: Eustigmatophyte microalgae are
1207 potential sources of C29 sterols, C22–C28 n-alcohols and C28–C32 n-alkyl diols
1208 in freshwater environments, Organic Geochemistry, 30, 307-318, 1999.

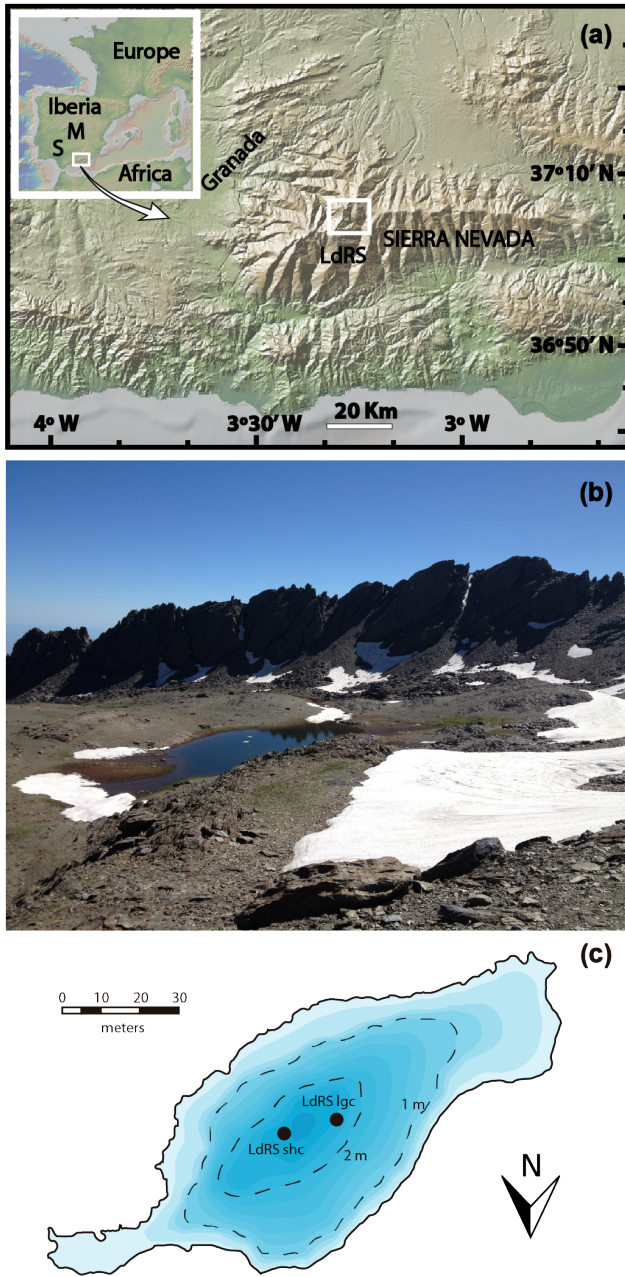
1209 Waters, C. N., Zalasiewicz, J., Summerhayes, C., Barnosky, A. D., Poirier, C.,
1210 Gałuszka, A., Cearreta, A., Edgeworth, M., Ellis, E. C., Ellis, M., Jeandel, C.,
1211 Leinfelder, R., McNeill, J. R., Richter, D. d., Steffen, W., Syvitski, J., Vidas, D.,

1212 Wagreeich, M., Williams, M., Zhisheng, A., Grinevald, J., Odada, E., Oreskes, N.,
1213 and Wolfe, A. P.: The Anthropocene is functionally and stratigraphically distinct
1214 from the Holocene, *Science*, 351, 2016.

1215 Willmott, V., Rampen, S. W., Domack, E., Canals, M., Sinninghe Damsté, J. S., and
1216 Schouten, S.: Holocene changes in *Proboscia* diatom productivity in shelf waters
1217 of the north-western Antarctic Peninsula, *Antarctic Science*, 22, 3-10, 2010.

1218 Yu, M., Zhang, H., Li, L., and Zhao, M.: Spatial Distributions and Potential Sources of
1219 Long Chain (C30, C32 1,15-) Alkyl Diols in Surface Sediments from Eastern
1220 China Marginal Seas, *Journal of Ocean University of China*, 17, 1114-1122, 2018.

1221



1223

1224 **Figure 1. Geographical setting.** (a) Location of the Sierra Nevada in the western
 1225 Mediterranean region, Madrid (M), Sevilla (S) and Granada observatories, as well as the
 1226 studied area: Laguna de Río Seco (LdRS), (b) LdRS catchment basin (0.42 ha) in spring
 1227 2013, (c) bathymetry map of LdRS along with the sampling points of both cores. Data
 1228 source and software: (a) map created by A. García-Alix using GeoMapApp (3.6.6)
 1229 (<http://www.geomapp.org>), (b) picture from A. García-Alix, (c) digitalized map of a
 1230 bathymetry report from Egmasa S.A.

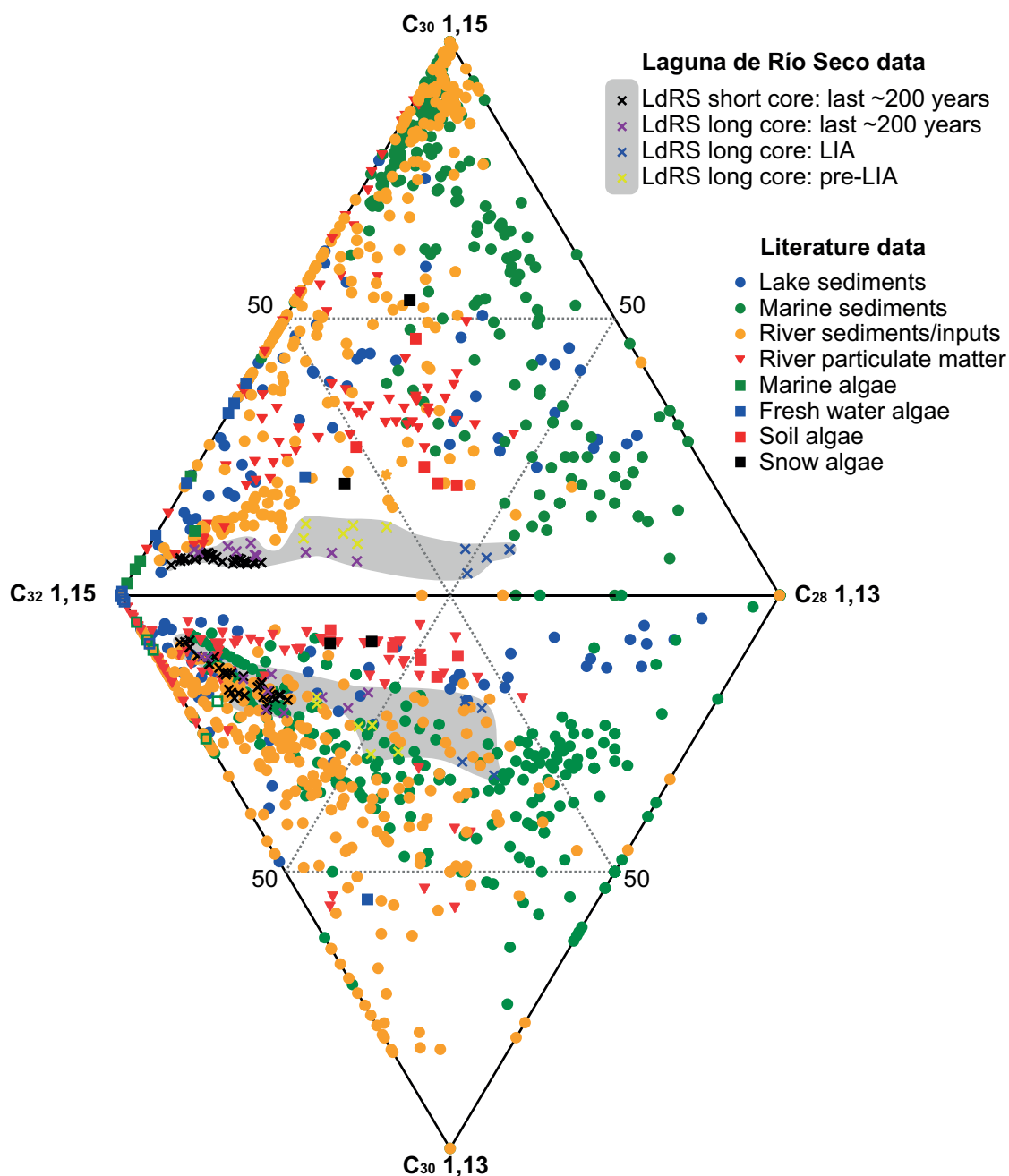
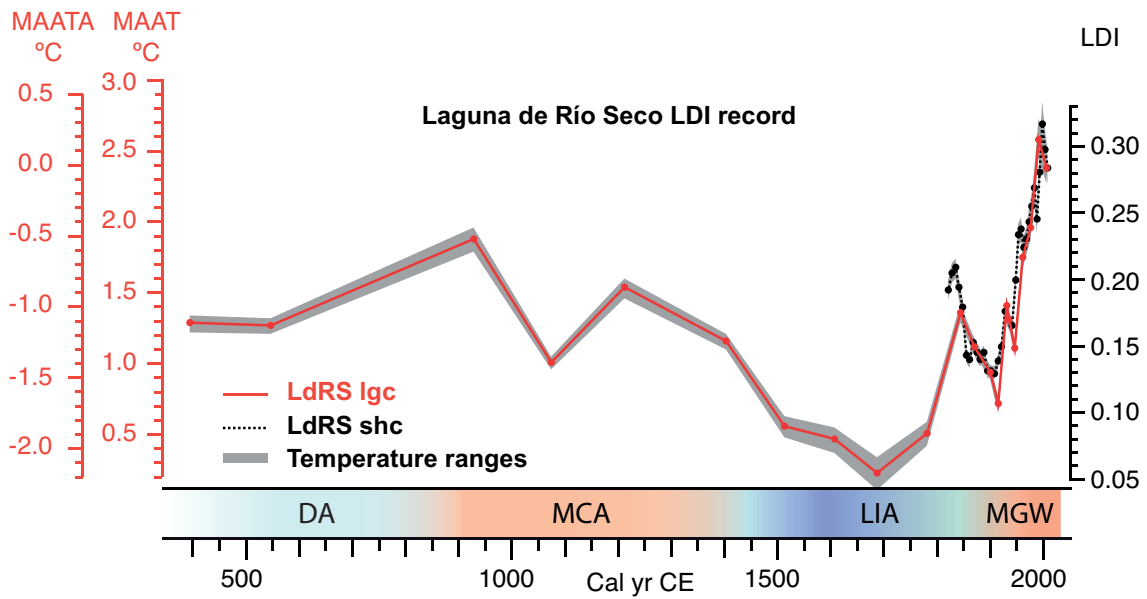
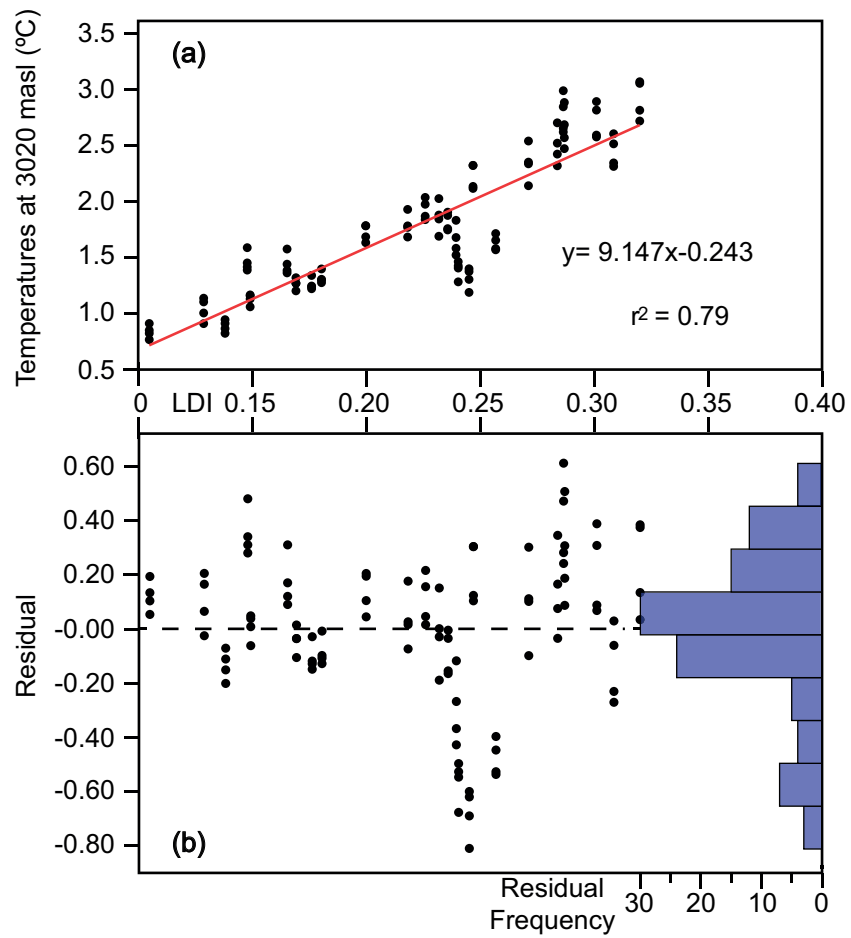


Figure 2. Double-ternary diagram of the relative abundances of C₂₈ 1,13-diol, C₃₀ 1,13-diol, C₃₀ 1,15-diol, and C₃₂ 1,15-diol from LdRS short core (LdRS shc ~200 years) and LdRS long core (LdRS lgc ~1500 years). Diol data compiled from the literature: lake sediments (Rampen et al., 2014a), algal cultures (Rampen et al., 2014a), marine sediments (de Bar et al., 2016; Lattaud et al., 2017a; Rampen et al., 2014b; Rampen et al., 2012), river sediments/inputs (de Bar et al., 2016; Lattaud et al., 2017b), river particulate organic matter (Lattaud et al., 2018a).



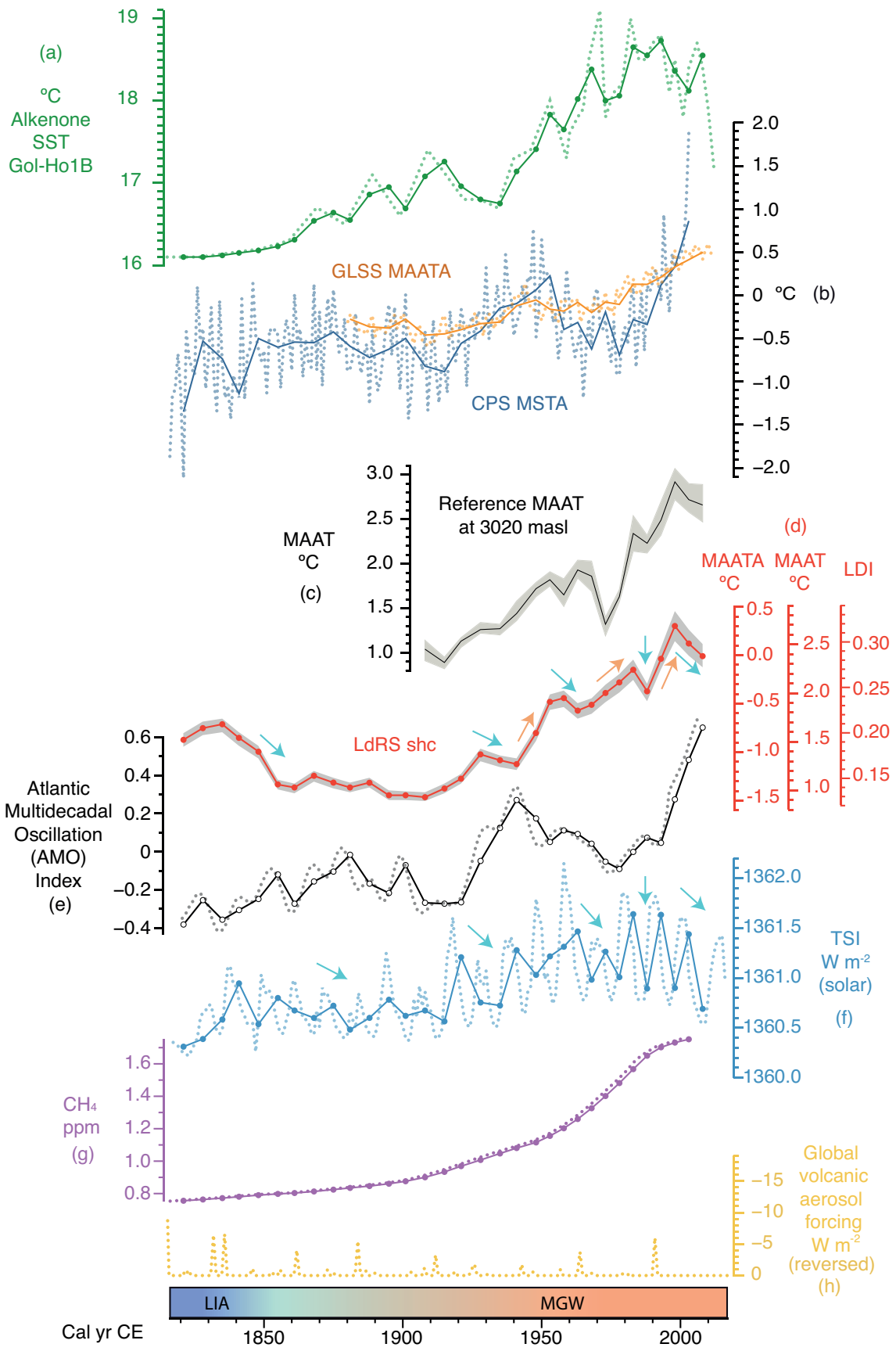
1239

1240 **Figure 3.** LDI record from LdRS, including both long core (solid line) and short core
 1241 (dashed line), mean annual air temperature (MAAT °C) reconstruction from LDI records
 1242 of LdRS, as well as mean annual air temperature anomaly reconstruction (MAATA°C)
 1243 respect to the annual MAAT of the last 30 years (1979-2008). The grey shade shows the
 1244 reconstructed maximum and minimum temperature ranges obtained from the four LDI
 1245 individual calibrations.

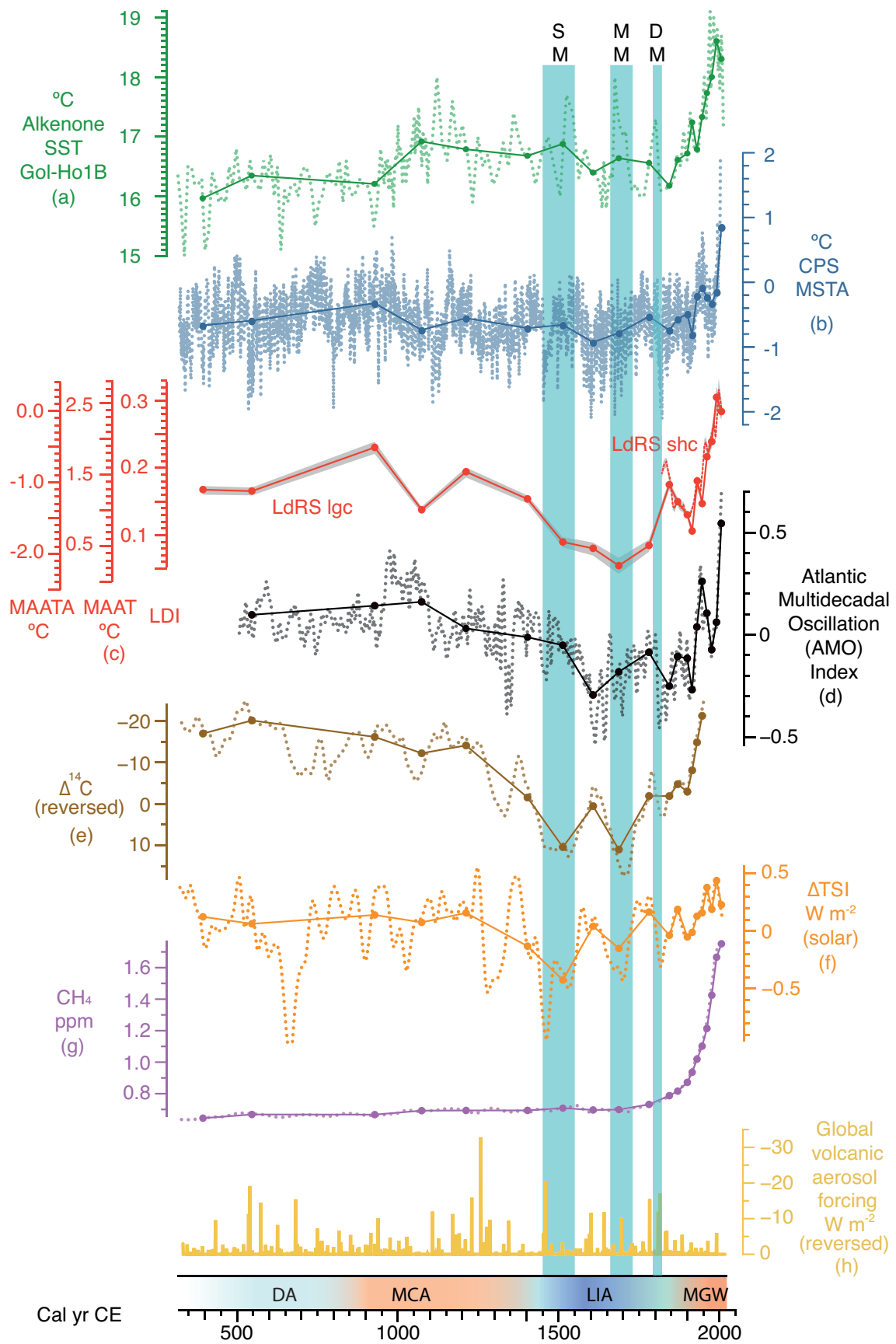


1246
1247

1248 **Figure 4. LDI temperature calibration.** (a) Correlations by means of ordinary least
 1249 square regression between the **both** LDI records from LdRS (**from 1908 to 2008**) and the
 1250 four reference temperature time-series at 3020 **masl**. (b) LDI values of LdRS vs residual
 1251 temperatures (calculated between the calibrated LDI temperatures vs reference
 1252 temperature time series at 3020 masl), as well as the histogram of the frequency of these
 1253 residuals.



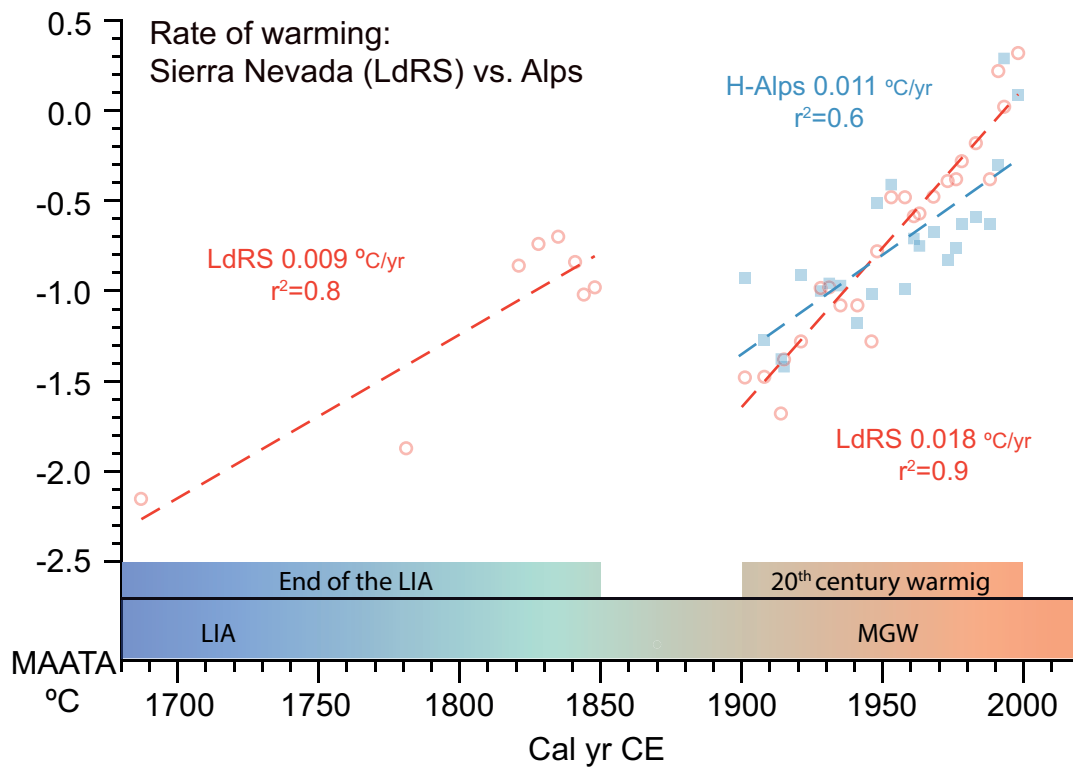
1255 **Figure 5. Comparison of the LDI record and the reconstructed temperatures for the**
1256 **last ~200 years of LdRS with marine and terrestrial temperature records, Atlantic**
1257 **multidecadal oscillations, greenhouse gases, solar radiation and volcanic eruption**
1258 **records.** Original data are in dashed lines. Solid lines represent the same time averaging
1259 as the LDI data in LdRS shc (data were linearly interpolated and time-averaged to the
1260 same resolution as the sampling points of LdRS shc) to facilitate the correlation. (a)
1261 Alkenone-derived Sea Surface Temperatures (SST, °C) of the core Gol-Ho1B_KSGC-31
1262 (Gulf of Lion: NW Mediterranean Sea ([Sicre et al., 2016](#))), (b) Composite-plus-scaling
1263 (CPS) mean summer temperature anomaly reconstruction from tree rings records in
1264 Europe with respect to 1974-2003 (MSTA °C) ([Luterbacher et al., 2016](#)) as well as global
1265 land and sea surface (GLSS) mean annual temperature anomalies with respect to 1979-
1266 2008 CE (MAATA °C) ([Hansen et al., 2010](#)), (c) Summary of the four reference
1267 temperature time-series at 3020 masl: grey shade show the maximum and minimum
1268 temperature range and the black solid line represent the mean temperature values, (d) LDI
1269 record along with reconstructed mean annual air temperatures (MAAT °C) and mean
1270 annual air temperature anomalies with respect to 1979-2008 CE (MAATA °C) for the last
1271 ~200 years in LdRS, (e) Atlantic Multidecadal Oscillation (AMO) reconstruction ([Mann](#)
1272 [et al., 2009](#)), (f) high resolution total solar irradiance reconstruction (TSI, W m⁻²)
1273 ([Coddington et al., 2016](#)), (g) reconstructed concentration of atmospheric CH₄ (ppm)
1274 ([Schmidt et al., 2011](#)), and (h) reconstruction of the global volcanic aerosol forcing (W
1275 m⁻²) (reversed) ([Sigl et al., 2015](#)). Acronyms: LIA, Little Ice Age; MGW, Modern Global
1276 Warming. Blue arrows: decrease; orange arrows: increase.




1278 **Figure 6. Comparison of the LDI record and the reconstructed temperatures for the**
1279 **last ~1500 years of LdRS with marine and terrestrial temperature records, Atlantic**
1280 **multidecadal oscillations, solar radiation, greenhouse gases, and volcanic eruption**
1281 **records.** Original data are in dashed lines. Solid dots represent the same time averaging
1282 as the LDI data in LdRS lgc (data were linearly interpolated and time-averaged to the
1283 same resolution as the sampling points of LdRS lgc) to facilitate the Pearson correlation:
1284 **(a)** Alkenone-Sea Surface Temperatures (SST, °C) of the core Gol-Ho1B_KSGC-31
1285 (Gulf of Lion: NW Mediterranean Sea ([Sicre et al., 2016](#))), **(b)** Composite-plus-scaling
1286 (CPS) mean summer temperature anomaly reconstruction from tree rings records in
1287 Europe with respect to 1974-2003 CE (MSTA °C) ([Luterbacher et al., 2016](#)), **(c)** LDI
1288 record along with reconstructed mean annual air temperatures (MAAT °C) and mean
1289 annual air temperature anomalies with respect to 1979-2008 CE (MAATA °C) for the last
1290 1500 years in LdRS, **(d)** Atlantic Multidecadal Oscillation (AMO) reconstruction ([Mann](#)
1291 [et al., 2009](#)), **(e)** $\Delta^{14}\text{C}$ in the atmosphere (reversed) ([Reimer et al., 2013](#)), **(f)** reconstruction
1292 of the difference of the total solar irradiance from the value of the PMOD composite
1293 series during the solar cycle minimum of the year 1986 CE (1365.57 W m^{-2}) (ΔTSI)
1294 ([Steinhilber et al., 2009](#)), **(g)** reconstructed concentration of atmospheric CH_4 (ppm)
1295 ([Schmidt et al., 2011](#)), and **(h)** reconstruction of the global volcanic aerosol forcing (W
1296 m^{-2}) (reversed) ([Sigl et al., 2015](#)). Acronyms: DA, Dark Ages; MCA, Medieval Climate
1297 Anomaly; LIA, Little Ice Age; MGW, Modern Global Warming. Blue bars show three
1298 low solar activity periods, the Spörer Minimum (SM), the Maunder Minimum (MM), and
1299 the Dalton Minimum (DM).

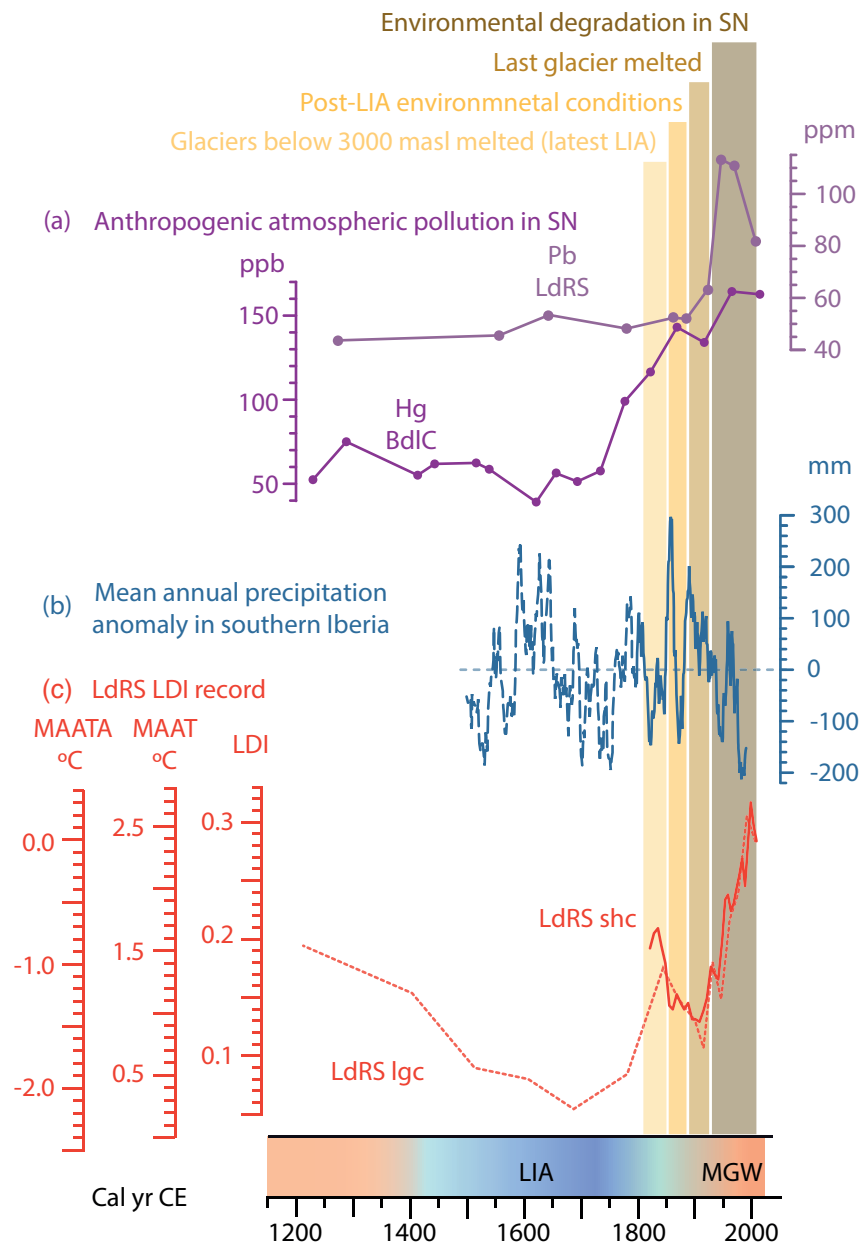
1300

1301



1302

1303 **Figure 7.** Comparison  between the average temperature warming rates from LdRS
 1304 and the alpine areas of the Alps by means of ordinary least square regressions. LDI-
 1305 deduced MAATA (respect to the period 1979-2008 CE) from LdRS long and short cores
 1306 for the last stage of the LIA and the 20th century (red open circles), and high-Alps
 1307 historical (homogenised) temperature records from the Historical Instrumental
 1308 Climatological Surface Time Series of the Greater Alpine Region (HISTALP) database
 1309 ([Auer et al., 2007](#); [Böhm et al., 2010](#)) at the same time averaging as LdRS shc-lgc to
 1310 facilitate the comparison (blue closed squares).



1311

1312 **Figure 8. Comparison among different factors affecting the environmental evolution**

1313 **of alpine wetlands in the Sierra Nevada. (a)** records of anthropogenic heavy metal

1314 atmospheric pollution (Pb and Hg) in two alpine sites of the Sierra Nevada: Laguna de

1315 Río Seco (LdRS) and Borreguil de la Caldera (BdIC) ([Garcia-Alix et al., 2017](#); [Garcia-](#)

1316 [Alix et al., 2013](#)), **(b)** mean annual precipitation anomaly in southern Iberia from 1500 to

1317 1990 CE with respect to the mean value of the instrumental period (1791-1990 CE): solid

1318 line- instrumental data from Gibraltar (southern Iberia); dashed line- anomaly

1319 precipitation reconstruction ([Rodrigo et al., 1999](#)), **(c)** LDI and **reconstructed**

1320 temperatures in LdRS. Colour bars indicate the four main environmental stages in the
1321 Sierra Nevada (SN) during the last 200 years. Acronyms: LIA, Little Ice Age; MGW,
1322 Modern Global Warming.